Estimation of failure probability function under imprecise probabilities by active learning augmented probabilistic integration

Chao Dang[1], Pengfei Wei[2], Jingwen Song[3], and Michael Beer, M.ASCE[4]

[1]Doctoral Student, Institute for Risk and Reliability, Leibniz University Hannover, Callinstr. 34, Hannover 30167, Germany. Email: chao.dang@irz.uni-hannover.de

[2]Associate Professor, School of Mechanics, Civil Engineering and Architecture, Northwestern Polytechnical University, Xian 710072, PR China. (corresponding author). Email: pengfeiwei@nwpu.edu.cn

[3]Research Assistant Professor, Advanced Research Laboratories, Tokyo City University, 1-28-1 Tamazutsumi Setagaya-ku, Tokyo 158-8557, Japan. Email: song@tcu.ac.jp

[4]Professor, Institute for Risk and Reliability, Leibniz University Hannover, Callinstr. 34, Hannover 30167, Germany; Institute for Risk and Uncertainty, University of Liverpool, Peach Street, Liverpool L69 7ZF, United Kingdom; International Joint Research Center for Engineering Reliability and Stochastic Mechanics, Tongji University, Shanghai 200092, PR China. Email: beer@irz.uni-hannover.de

ABSTRACT

Imprecise probabilities have gained increasing popularity for quantitatively modelling uncertainty under incomplete information, which is usually encountered in engineering analysis. In this contribution, a non-intrusive method, termed as '*Active Learning Augmented Probabilistic Integration*' (ALAPI), is developed to efficiently estimate the failure probability function (FPF) in the presence of imprecise probabilities. Specially, the parameterized probability-box models are of specific concern. By interpreting the failure probability integral from a Bayesian probabilistic integration perspective, the discretization error can be regarded as a kind of epistemic uncertainty,

allowing it to be properly quantified and propagated through computational pipelines. Accordingly, an active learning probabilistic integration (ALPI) method is developed for failure probability estimation, in which a new learning function and a new stopping criterion associated with the upper bound of the posterior variance are proposed. Based on the idea of constructing an augmented uncertainty space, an imprecise augmented stochastic simulation (IASS) method is devised by using the RS-HDMR (random sampling high-dimensional representation model) for estimating the failure probability function in a pointwise stochastic simulation manner. To further improve the efficiency of IASS, the ALAPI is formed by an elegant combination of the ALPI and IASS, allowing the RS-HDMR component functions of the FPF to be properly inferred. Three benchmark examples are investigated to demonstrate the accuracy and efficiency of the proposed method.
Keywords: Failure probability function; Imprecise probability; Probability box; Gaussian process regression; Active learning; Bayesian probabilistic integration

INTRODUCTION

Uncertainty quantification and propagation have been essentially important, but still face critical challenges in many fields of science and engineering. This is because that in the real world, uncertainty is almost inevitable, and generally arises from a variety of distinct sources, e.g., statistical variability, measurement errors, instrumental uncertainty, imperfect information, limited data, abstraction and assumptions among others. Typically, these uncertainties can be categorized as either aleatory or epistemic according to their intrinsic features and effects on analysis (Der Kiureghian and Ditlevsen 2009; Beer et al. 2013). Aleatory uncertainty is related to the inherent randomness of an event or a parameter, and hence cannot be reduced even when sufficient information of high quality is available. On the contrary, epistemic uncertainty is due to a lack of knowledge, which therefore can be reduced by gaining more knowledge. In real-world applications, both kinds of uncertainties tend to be jointly present and are often easily confused with each other. As has been concluded by Der Kiureghian and Ditlevsen (Der Kiureghian and Ditlevsen 2009), without properly distinguishing different types of uncertainties, the results on risk and reliability analysis can be misleading.

As for the uncertainty representation, a large number of mathematical models have long been developed for quantitative characterization of uncertain phenomena in engineering practices. Generally, the existing uncertainty characterization models can be classified under three major frameworks: precise probability framework, non-probabilistic framework, and imprecise probability framework. The precise probability framework is deeply rooted in the well-established probability theory, and hence it is an essential tool in the quantitative mathematical treatment of uncertainty, especially for modelling aleatory uncertainty. A common criticism, however, is that large amounts of high-quality data are often required for inferring the potential precise probability model with sufficient credibility, which, unfortunately, may be rarely available for most engineering applications (Der Kiureghian and Ditlevsen 2009; Beer et al. 2013). Alternatively, some representative models within the non-probabilistic framework, such as interval model (Faes and Moens 2019), convex model (Jiang et al. 2013), fuzzy set theory (Möller and Beer 2004) among others, have been extensively investigated to describe the non-probabilistic uncertainty, especially those resulted from limited data with poor quality. In spite of their popularity, it has been argued that non-probabilistic models commonly fail to distinguish between the aleatory and epistemic uncertainties (Wei et al. 2019a). To fill this gap, the imprecise probability framework, mathematically as a combination of the non-probabilistic and probability frameworks, and physically making a clear separation of the two types of uncertainties, has gained increasingly attraction. Typical imprecise probability models include the evidence theory (Sentz et al. 2002), interval probabilities (Yager and Kreinovich 1999), probability-box (p-box) (Sun et al. 2012), fuzzy probabilities (Buckley 2005), etc. A novel character of imprecise probability framework is that it enables the aleatory uncertainty and epistemic uncertainty to be treated separately within a unified framework, thanks to the hierarchical model structure. Based on the aforementioned considerations, we are mainly focusing on propagating uncertainty in the form of imprecise probabilities in the present paper.

In the imprecise probability framework, uncertainty propagation through computer simulators is a computationally challenging task primarily due to the double-layer structure inherent in imprecise probability models. To address this challenge, there has been an increasing attention on developing

efficient numerical methods in recent years, which can be divided into two categories according to whether the method is decoupled or not. Typical coupled method includes the interval (quasi-) Monte Carlo simulation (Zhang et al. 2010; Zhang et al. 2013), interval importance sampling (Zhang 2012), subset simulation based method (Alvarez et al. 2018), method of moments (Liu et al. 2018; Liu et al. 2019), ect. Very often these coupled methods involve interval finite element analysis or numerical optimization within a nested loop, which still leads to high computational cost and limited applicability. For this reason, decoupled methods have drawn increasingly attention for propagating imprecise probabilities, such as the augmented subset simulation (ASS) (Au 2005), extended Monte Carlo simulation (Wei et al. 2014), non-intrusive imprecise stochastic simulation (NISS) (Wei et al. 2019a; Wei et al. 2019b; Song et al. 2020a; Song et al. 2020c), augmented line sampling (Yuan et al. 2020), operator norm theory (Faes et al. 2020; Faes et al. 2021b), augmented space integral (Yuan et al. 2021; Faes et al. 2021a). The most attractive feature of these methods is that only one simulation run is usually required, and hence very computationally efficient. Despite this, there still exist some respective drawbacks for those methods. For example, the NISS may not work well for problems with relatively large epistemic uncertainty due to the increasing variations of the NISS estimators; the application of operator norm theory is still limited to linear models with imprecision presented only in excitations; the augmented space integral is suffered from dimensionality of the epistemic parameters. To tackle the former issue, Wei and his co-workers (Wei et al. 2021) recently proposed a novel imprecise probability propagation framework, termed as non-intrusive imprecise probabilistic integration (NIPI). In this framework, the estimation of response moment function (RMF) is treated as a Bayesian inference problem in the augmented space, and estimators for the component functions of RMF are analytically derived in closed form. Remarkably, it has been shown that the NIPI can be applied to the problems with large epistemic uncertainty resulted from extreme lack of information. However, the current NIPI method is only capable of evaluating RMF, and for FPF estimation, further developments need to be presented as will be shown in this work.

The main objective of this paper is to develop a new non-intrusive method, called 'Active Learn-

ing Augmented Probabilistic Integration', for estimation of FPF under imprecise probabilities. The core of the methodology is to interpret the failure probability integral from the perspective of Bayesian probabilistic integration, and hence the discretization error can be regarded as a kind of epistemic uncertainty. Through this treatment, the discretization error is propagated via the computational pipelines simultaneously together with the aleatory uncertainty and epistemic uncertainty present in the imprecise probability models, which is useful and important for developing an active learning strategy, and also for facilitating error assessment of the computational results. Besides, the approach also relies on an augmented idea that artificially constructs an augmented uncertainty space, enabling the propagation of two kinds of uncertainties to be fully decoupled. At last, the RS-HDMR (random sampling high-dimensional model representation) is employed to study the functional form of the FPF by decomposing it as a summation of component functions of increased orders, through which, the failure probability bounds and sensitivity analysis can also be obtained as byproducts.

The rest of this paper is arranged as follows. The problem to be solved in this work is briefly stated in the "Problem Statement" section. The "Active Learning Augmented Probabilistic Integration" section provides the detailed theoretical background and numerical implementation procedure of the proposed method. In the "Numerical Examples" section, three numerical examples are studied to verify the proposed method. The "Conclusions" section gives the findings of the present study.

PROBLEM STATEMENT

Let the limit state function (also termed as performance function) of a physical system under consideration be denoted by a deterministic mapping $y = g(\boldsymbol{x})$, which is referred to as g-function hereinafter. Under this setting, the uncertainty in y only results from the uncertainty in $\boldsymbol{x}$, where $\boldsymbol{x} = [x_1, x_2, \ldots, x_n]$ is the n-dimensional row vector of input random variables that reflects the aleatory uncertainty of model inputs. In this paper, we only consider the case that each input random variable is characterized by a parameterized probability-box (p-box). Let $f(\boldsymbol{x}|\boldsymbol{\theta})$ denote the joint probability density function (PDF) of $\boldsymbol{x}$, which is conditional on its distribution parameters

$\boldsymbol{\theta} = [\theta_1, \theta_2, \ldots, \theta_m]$. Due to the epistemic uncertainty, the distribution parameters cannot be precisely known, but also uncertain. For simplicity, the interval model is employed to characterize the uncertainty of $\boldsymbol{\theta}$, i.e., $\boldsymbol{\theta} \in \left[\underline{\boldsymbol{\theta}}, \bar{\boldsymbol{\theta}}\right]$, where $\underline{\boldsymbol{\theta}} = [\underline{\theta}_1, \underline{\theta}_2, \ldots, \underline{\theta}_m]$ and $\bar{\boldsymbol{\theta}} = [\bar{\theta}_1, \bar{\theta}_2, \ldots, \bar{\theta}_m]$ are the lower bound and upper bound, respectively. Besides, it is assumed that all the random variables and the distribution parameters are mutually independent. The output y is a state variable with $y \leq 0$ indicating that the system is failed, and safe otherwise. The FPF is expressed as:

$$P_f(\boldsymbol{\theta}) = \int_{\mathcal{X}} I_F(\boldsymbol{x}) f(\boldsymbol{x}|\boldsymbol{\theta}) \mathrm{d}\boldsymbol{x}, \tag{1}$$

where F in the subscript denotes the failure domain defined as $F = \{\boldsymbol{x} : g(\boldsymbol{x}) \leq 0\}$; $I_F(\boldsymbol{x})$ is an indicator function of failure: if $\boldsymbol{x} \in F$, $I_F(\boldsymbol{x}) = 1$, and $I_F(\boldsymbol{x}) = 0$ otherwise.

The main objective of this work is to evaluate the FPF defined by a integral with $\boldsymbol{\theta}$ being its argument. This is a more general task than calculating the failure probability bounds, since, with it, the failure probability bounds can be easily obtained without extra g-function evaluations. Besides, FPF also provides a basis for sensitivity analysis (Wei et al. 2018) and reliability-based design optimization (Liu and Cheung 2017; Ling et al. 2020). In most practical cases, however, the closed-form solution of the integral is not available because of the underlying complexity of the problem at hand. Alternatively, numerical techniques are thus especially desirable for more general applications.

ACTIVE LEARNING AUGMENTED PROBABILISTIC INTEGRATION (ALAPI)

In this section, we propose a method, termed as "active learning augmented probabilistic integration" (ALAPI), for efficiently propagating the p-box models and evaluating the failure probability function. The method starts by interpreting the estimation of failure probability integral with Bayesian inference, instead of a purely frequentist view. This will enable to incorporate our prior knowledge about the g-function and the possibility of an adaptive experimental design so as to develop an active learning probabilistic integration (ALPI) framework. Based on the idea of augmented uncertainty space, an imprecise augmented stochastic simulation (IASS) method is

proposed to estimate the FPF in a pointwise stochastic simulation manner by utilizing the RS-HDMR. At last, the ALAPI is developed by an elegant combination of the ALPI and IASS.

Bayesian failure probability estimation: Active learning probabilistic integration (ALPI)

For brevity and convenience, let us first consider the case that $\boldsymbol{\theta}$ is precisely known and takes a fixed value $\boldsymbol{\theta}^\star$. That is, $f(\boldsymbol{x}|\boldsymbol{\theta}^\star)$ is now reduced to be a precise probability model. Under this setting, the failure probability should be a constant value from a theoretical standpoint, and expressed as:

$$P_f^\star = \int_{\mathcal{X}} I_F(\boldsymbol{x}) f(\boldsymbol{x}|\boldsymbol{\theta}^\star) \mathrm{d}\boldsymbol{x}. \tag{2}$$

As mentioned earlier, in most cases analytical derivation of the exact value of $P_f^\star$ is computationally intractable and even impossible, and usually we have to resort to numerical integration techniques for a crude estimate. Therefore, the introduction of error is unavoidable because the discretisation of the integrand is numerically necessary. Different from the frequentist theory of inference, we seek to reinterpret the problem of evaluating the failure probability integral in Eq. (2) via Bayesian inference, which is commonly known as Bayesian Quadrature (or Bayesian Probabilistic Integration) (O'Hagan 1991; Rasmussen and Ghahramani 2003; Briol et al. 2019; Wei et al. 2020). A novel feature of this treatment is that the discretisation error can be characterized as a kind of epistemic uncertainty, and then propagated through computational pipelines. One should not be confused with two kinds of epistemic uncertainties mentioned so far. One is the epistemic uncertainty here in the probabilistic integration, which arises from the computation due to the discretisation error. This is in contrast to the epistemic uncertainty revealed in the distribution parameters of input random variables, which comes from the computation setup, rather than the computation itself. In the framework of probabilistic integration, the integrand $I_F(\boldsymbol{x})$ at any fixed $\boldsymbol{x}$ is seen as a random variable simply because it is numerically unknown until we actually evaluate it. This is usually the case since $I_F(\boldsymbol{x})$ is computationally expensive, and we cannot afford to compute $I_F(\boldsymbol{x})$ (or equivalently $g(\boldsymbol{x})$) at every site. Following a standard Bayesian approach, one needs to first assign a prior probability measure over the integrand $I_F(\boldsymbol{x})$, which expresses the

investigator's prior beliefs about the actual function value. Conditioning on the limited observations $\left\{\boldsymbol{x}^{(i)}, I_F^{(i)}(\boldsymbol{x}^{(i)})\right\}_{i=1}^{d}$, we can obtain a posterior over $I_F(\boldsymbol{x})$ via Bayes rule. This in turn will imply a posterior distribution over $P_f^\star$, which reflects the epistemic uncertainty resulted from the fact that we can only evaluate the integrand at a finite number of inputs.

The Gaussian process (GP) could be the most popular choice for the prior model, due to its broad applicability and sound theoretical background. However, we argue that it is inappropriate to directly specify a GP prior over the failure indicator function $I_F(\boldsymbol{x})$, since we know that it is discontinuous and actually follows a Bernoulli distribution. Alternatively, we put a GP prior over the performance function $g(\boldsymbol{x})$, denoted by

$$\hat{g}(\boldsymbol{x}) \sim \mathcal{GP}(\mu(\boldsymbol{x}), c(\boldsymbol{x}, \boldsymbol{x}')), \tag{3}$$

where $\mu(\boldsymbol{x})$ is the prior expectation function and $c(\boldsymbol{x}, \boldsymbol{x}')$ is the prior covariance function (also called kernel function). Various kinds of explicit functions with several hyper-parameters to be determined are available for the expectation function and covariance function in the literature. For more details, one can refer to (Rasmussen 2003; Murphy 2012).

Given the experimental design matrix $\boldsymbol{X} = \{\boldsymbol{x}^{(i)}\}_{i=1}^{d}$ of size $d \times n$ and the corresponding response vector $Y = \{y^{(i)} = g(\boldsymbol{x}^{(i)})\}_{i=1}^{d}$ of size $d \times 1$, the hyper-parameters involved in the prior mean function and covariance function can be specified, e.g., by using maximum likelihood estimation (Rasmussen 2003).

Conditional on the observed data set $\mathcal{D} = \{\boldsymbol{X}, Y\}$, the posterior prediction of $\hat{g}(\boldsymbol{x})$ at a new site $\boldsymbol{x}$ follows a Gaussian random variable with expectation and variance being

$$\mathbb{E}_{\mathcal{D}}[\hat{g}(\boldsymbol{x})] = \mu(\boldsymbol{x}) + \boldsymbol{c}(\boldsymbol{x}, \boldsymbol{X})^{\mathrm{T}} \boldsymbol{C}^{-1}(Y - \boldsymbol{\mu}(\boldsymbol{X})), \tag{4}$$

$$\mathbb{V}_{\mathcal{D}}[\hat{g}(\boldsymbol{x})] = c(\boldsymbol{x}, \boldsymbol{x}) - \boldsymbol{c}(\boldsymbol{x}, \boldsymbol{X})^{\mathrm{T}} \boldsymbol{C}^{-1} \boldsymbol{c}(\boldsymbol{x}, \boldsymbol{X}), \tag{5}$$

where $\mathbb{E}_{\mathcal{D}}[\cdot]$ and $\mathbb{V}_{\mathcal{D}}[\cdot]$ denote the posterior expectation and variance operators (a subscript "$\mathcal{D}$" is

used to indicate the posterior), receptively; $\boldsymbol{\mu}(\boldsymbol{X}) = [\mu(\boldsymbol{x}^{(1)}), \mu(\boldsymbol{x}^{(2)}), \ldots, \mu(\boldsymbol{x}^{(d)})]^{\mathrm{T}}$ is the mean vector; $\boldsymbol{c}(\boldsymbol{x}, \boldsymbol{X}) = [c(\boldsymbol{x}, \boldsymbol{x}^{(1)}), c(\boldsymbol{x}, \boldsymbol{x}^{(2)}), \ldots, c(\boldsymbol{x}, \boldsymbol{x}^{(d)})]^{\mathrm{T}}$ is the covariance vector between $\boldsymbol{x}$ and $\boldsymbol{X}$; $\boldsymbol{C}$ is the covariance matrix of $\boldsymbol{X}$ with entry $[\boldsymbol{C}]_{ij} = c(\boldsymbol{x}^{(i)}, \boldsymbol{x}^{(j)})$.

Based on the Gaussian posterior of $\hat{g}(\boldsymbol{x})$, it is easy to know that the posterior stochastic process $\hat{I}_F(\boldsymbol{x})$ at site $\boldsymbol{x}$ is a Bernoulli random variable with

$$\mathbb{P}_{\mathcal{D}}[\hat{I}_F(\boldsymbol{x}) = 1] = \mathbb{P}_{\mathcal{D}}[\hat{g}(\boldsymbol{x}) \leq 0] = \Phi\left(\frac{-\mathbb{E}_{\mathcal{D}}[\hat{g}(\boldsymbol{x})]}{\sqrt{\mathbb{V}_{\mathcal{D}}[\hat{g}(\boldsymbol{x})]}}\right), \tag{6}$$

$$\mathbb{P}_{\mathcal{D}}[\hat{I}_F(\boldsymbol{x}) = 0] = \mathbb{P}_{\mathcal{D}}[\hat{g}(\boldsymbol{x}) > 0] = 1 - \Phi\left(\frac{0 - \mathbb{E}_{\mathcal{D}}[\hat{g}(\boldsymbol{x})]}{\sqrt{\mathbb{V}_{\mathcal{D}}[\hat{g}(\boldsymbol{x})]}}\right) = \Phi\left(\frac{\mathbb{E}_{\mathcal{D}}[\hat{g}(\boldsymbol{x})]}{\sqrt{\mathbb{V}_{\mathcal{D}}[\hat{g}(\boldsymbol{x})]}}\right), \tag{7}$$

where $\mathbb{P}_{\mathcal{D}}[\cdot]$ denotes the posterior probability operator; Φ is the cumulative distribution function (CDF) of the standard normal variable.

Accordingly, the posterior expectation and variance of $\hat{I}_F(\boldsymbol{x})$ at site $\boldsymbol{x}$ are formulated as:

$$\mathbb{E}_{\mathcal{D}}[\hat{I}_F(\boldsymbol{x})] = \Phi\left(\frac{-\mathbb{E}_{\mathcal{D}}[\hat{g}(\boldsymbol{x})]}{\sqrt{\mathbb{V}_{\mathcal{D}}[\hat{g}(\boldsymbol{x})]}}\right), \tag{8}$$

and

$$\mathbb{V}_{\mathcal{D}}[\hat{I}_F(\boldsymbol{x})] = \Phi\left(\frac{-\mathbb{E}_{\mathcal{D}}[\hat{g}(\boldsymbol{x})]}{\sqrt{\mathbb{V}_{\mathcal{D}}[\hat{g}(\boldsymbol{x})]}}\right)\Phi\left(\frac{\mathbb{E}_{\mathcal{D}}[\hat{g}(\boldsymbol{x})]}{\sqrt{\mathbb{V}_{\mathcal{D}}[\hat{g}(\boldsymbol{x})]}}\right). \tag{9}$$

Rewrite the failure probability integral in Eq.(2) as:

$$\hat{P}_f^{\star} = \int_{\mathcal{X}} \hat{I}_F(\boldsymbol{x}) f(\boldsymbol{x}|\boldsymbol{\theta}^{\star}) \mathrm{d}\boldsymbol{x}. \tag{10}$$

Since the integral above is just a linear projection of $\hat{I}_F(\boldsymbol{x})$, the posterior of $\hat{P}_f^{\star}$ is also random with

expectation and variance being:

$$\begin{aligned}\mathbb{E}_{\mathcal{D}}[\hat{P}_f^\star] &= \mathbb{E}_{\mathcal{D}}\left[\int_{\mathcal{X}} \hat{I}_F(\boldsymbol{x}) f(\boldsymbol{x}|\boldsymbol{\theta}^\star)\mathrm{d}\boldsymbol{x}\right] \\ &= \int_{\mathcal{X}} \mathbb{E}_{\mathcal{D}}[\hat{I}_F(\boldsymbol{x})] f(\boldsymbol{x}|\boldsymbol{\theta}^\star)\mathrm{d}\boldsymbol{x} \\ &= \int_{\mathcal{X}} \Phi\left(\frac{-\mathbb{E}_{\mathcal{D}}[\hat{g}(\boldsymbol{x})]}{\sqrt{\mathbb{V}_{\mathcal{D}}[\hat{g}(\boldsymbol{x})]}}\right) f(\boldsymbol{x}|\boldsymbol{\theta}^\star)\mathrm{d}\boldsymbol{x} \\ &= \mathbb{E}_{\mathcal{X}}\left[\Phi\left(\frac{-\mathbb{E}_{\mathcal{D}}[\hat{g}(\boldsymbol{x})]}{\sqrt{\mathbb{V}_{\mathcal{D}}[\hat{g}(\boldsymbol{x})]}}\right)\right],\end{aligned} \tag{11}$$

and

$$\begin{aligned}\mathbb{V}_{\mathcal{D}}[\hat{P}_f^\star] =& \mathbb{E}_{\mathcal{D}}\left[\left(\hat{P}_f^\star - \mathbb{E}_{\mathcal{D}}[\hat{P}_f^\star]\right)^2\right] \\ =& \mathbb{E}_{\mathcal{D}}\left[\left(\int_{\mathcal{X}} \hat{I}_F(\boldsymbol{x}) f(\boldsymbol{x}|\boldsymbol{\theta}^\star)\mathrm{d}\boldsymbol{x} - \int_{\mathcal{X}} \mathbb{E}_{\mathcal{D}}[\hat{I}_F(\boldsymbol{x})] f(\boldsymbol{x}|\boldsymbol{\theta}^\star)\mathrm{d}\boldsymbol{x}\right)^2\right] \\ =& \mathbb{E}_{\mathcal{D}}\left[\left(\int_{\mathcal{X}} \left(\hat{I}_F(\boldsymbol{x}) - \mathbb{E}_{\mathcal{D}}[\hat{I}_F(\boldsymbol{x})]\right) f(\boldsymbol{x}|\boldsymbol{\theta}^\star)\mathrm{d}\boldsymbol{x}\right)^2\right] \\ =& \mathbb{E}_{\mathcal{D}}\left[\left(\int_{\mathcal{X}} \left(\hat{I}_F(\boldsymbol{x}) - \mathbb{E}_{\mathcal{D}}[\hat{I}_F(\boldsymbol{x})]\right) f(\boldsymbol{x}|\boldsymbol{\theta}^\star)\mathrm{d}\boldsymbol{x}\right)\left(\int_{\mathcal{X}} \left(\hat{I}_F(\boldsymbol{x}') - \mathbb{E}_{\mathcal{D}}[\hat{I}_F(\boldsymbol{x}')]\right) f(\boldsymbol{x}'|\boldsymbol{\theta}^\star)\mathrm{d}\boldsymbol{x}'\right)\right] \\ =& \int_{\mathcal{X}}\int_{\mathcal{X}} \mathbb{E}_{\mathcal{D}}\left[\left(\hat{I}_F(\boldsymbol{x}) - \mathbb{E}_{\mathcal{D}}[\hat{I}_F(\boldsymbol{x})]\right)\left(\hat{I}_F(\boldsymbol{x}') - \mathbb{E}_{\mathcal{D}}[\hat{I}_F(\boldsymbol{x}')]\right)\right] f\left(\boldsymbol{x}|\boldsymbol{\theta}^\star\right) f\left(\boldsymbol{x}'|\boldsymbol{\theta}^\star\right)\mathrm{d}\boldsymbol{x}\mathrm{d}\boldsymbol{x}' \\ =& \int_{\mathcal{X}}\int_{\mathcal{X}} \mathbb{COV}_{\mathcal{D}}[\hat{I}_F\left(\boldsymbol{x}\right), \hat{I}_F\left(\boldsymbol{x}'\right)] f\left(\boldsymbol{x}|\boldsymbol{\theta}^\star\right) f\left(\boldsymbol{x}'|\boldsymbol{\theta}^\star\right)\mathrm{d}\boldsymbol{x}\mathrm{d}\boldsymbol{x}',\end{aligned} \tag{12}$$

where $\mathbb{E}_{\mathcal{X}}[\cdot]$ is the expectation operator with respect to $\boldsymbol{x}$; the term $\mathbb{COV}_{\mathcal{D}}[\hat{I}_F\left(\boldsymbol{x}\right), \hat{I}_F\left(\boldsymbol{x}'\right)]$ is the posterior covariance between $\hat{I}_F(\boldsymbol{x})$ and $\hat{I}_F(\boldsymbol{x}')$, whose closed-form solution is not available.

It is reasonable to assume that $\hat{I}_F\left(\boldsymbol{x}\right)$ and $\hat{I}_F\left(\boldsymbol{x}'\right)$ have finite variances, and then the following inequality holds via the Cauchy-Schwarz inequality:

$$\mathbb{COV}_{\mathcal{D}}\left[\hat{I}_F\left(\boldsymbol{x}\right), \hat{I}_F\left(\boldsymbol{x}'\right)\right] \leq \sqrt{\mathbb{V}_{\mathcal{D}}[\hat{I}_F(\boldsymbol{x})]}\sqrt{\mathbb{V}_{\mathcal{D}}[\hat{I}_F(\boldsymbol{x}')]}. \tag{13}$$

Substituting Eq. (13) into Eq. (12), gives the upper bound of the posterior variance of $\hat{P}_f^\star$:

$$\begin{aligned}
\mathbb{V}_{\mathcal{D}}[\hat{P}_f^\star] &= \int_{\mathcal{X}}\int_{\mathcal{X}} \mathbb{COV}_{\mathcal{D}}[\hat{I}_F(\boldsymbol{x}), \hat{I}_F\left(\boldsymbol{x}^{'}\right)] f(\boldsymbol{x}|\boldsymbol{\theta}^\star)\, f\left(\boldsymbol{x}^{'}|\boldsymbol{\theta}^\star\right) \mathrm{d}\boldsymbol{x}\mathrm{d}\boldsymbol{x}^{'} \\
&\leq \int_{\mathcal{X}}\int_{\mathcal{X}} \sqrt{\mathbb{V}_{\mathcal{D}}[\hat{I}_F(\boldsymbol{x})]}\sqrt{\mathbb{V}_{\mathcal{D}}[\hat{I}_F(\boldsymbol{x}^{'})]} f(\boldsymbol{x}|\boldsymbol{\theta}^\star)\, f\left(\boldsymbol{x}^{'}|\boldsymbol{\theta}^\star\right) \mathrm{d}\boldsymbol{x}\mathrm{d}\boldsymbol{x}^{'} \\
&= \left(\int_{\mathcal{X}} \sqrt{\mathbb{V}_{\mathcal{D}}[\hat{I}_F(\boldsymbol{x})]} f(\boldsymbol{x}|\boldsymbol{\theta}^\star)\, \mathrm{d}\boldsymbol{x}\right)^2 \\
&= \left(\mathbb{E}_{\mathcal{X}}\left[\sqrt{\Phi\left(\frac{-\mathbb{E}_{\mathcal{D}}[\hat{g}(\boldsymbol{x})]}{\sqrt{\mathbb{V}_{\mathcal{D}}[\hat{g}(\boldsymbol{x})]}}\right)\Phi\left(\frac{\mathbb{E}_{\mathcal{D}}[\hat{g}(\boldsymbol{x})]}{\sqrt{\mathbb{V}_{\mathcal{D}}[\hat{g}(\boldsymbol{x})]}}\right)}\right]\right)^2 .
\end{aligned} \tag{14}$$

Note that similar equations with Eq. (11) and (14) have been available in the literature (e.g., (Dubourg et al. 2013; Bae et al. 2020)), but they are derived from other perspectives, rather than Bayesian probabilistic integration. The posterior expectation in Eq. (11) can be used as the estimator of the failure probability, and the upper bound of the posterior variance in Eq. (14) can measure the epistemic uncertainty of this estimator induced by the limited number of observations, but roughly since it might be magnified to a certain extent.

Adaptive experimental design

In order to accelerate the convergence of GP training process and increase the accuracy of failure probability predictor, a careful experimental design is required. It has been shown in the previous studies, e.g., AK-MCS (Echard et al. 2011), AK-IS (Echard et al. 2013), AK-MCMC (Wei et al. 2019c) and AGPR-LS (Song et al. 2020b), an adaptive experimental design strategy is very useful for building a accurate GP model at less computational expense. The key is to develop a suitable learning function (or called acquisition function) that can decide the next evaluation point based on the current GP model. Since the upper bound of the posterior variance of the failure probability integral has been derived in the previous subsection, it is hence possible for us to develop an adaptive experimental design so as to reduce the epistemic uncertainty of the failure probability predictor as much as possible.

For the above purposes, we will define a new learning function, called upper bound posterior

variance contribution (UPVC), which is given as follows:

$$\mathrm{UPVC}(\boldsymbol{x}) = \Phi\left(\frac{-\mathbb{E}_{\mathcal{D}}[\hat{g}(\boldsymbol{x})]}{\sqrt{\mathbb{V}_{\mathcal{D}}[\hat{g}(\boldsymbol{x})]}}\right)\Phi\left(\frac{\mathbb{E}_{\mathcal{D}}[\hat{g}(\boldsymbol{x})]}{\sqrt{\mathbb{V}_{\mathcal{D}}[\hat{g}(\boldsymbol{x})]}}\right), \tag{15}$$

which actually reflects the contribution of epistemic uncertainty at any site $\boldsymbol{x}$ to the upper bound of posterior variance of the failure probability predictor. If the point processing the largest UPVC value (i.e., $\boldsymbol{x}^\star = \arg\max_{\boldsymbol{x}} \mathrm{UPVC}(\boldsymbol{x})$) is sequentially added to the training data set $\mathcal{D}$, the upper bound of posterior variance of failure probability integral is expected to decrease most fastest, and hence we will obtain a more accurate prediction of failure probability at lower computational cost. Therefore, the active learning criterion proposed in this work is to find the maximum point of UPVC function, which is used as the best next point to evaluate on the real g-function.

In addition to the active learning criterion, a stopping criterion for indicating the convergence of the algorithm should also be presented. In this study, we propose a new stopping criterion, which is based on the judgment of the posterior coefficient of variation (COV) of failure probability predictor. In terms of Eqs. (11) and (14), the upper bound of the posterior COV of failure probability can be expressed as:

$$\kappa^\star = \overline{\mathbb{COV}}_{\mathcal{D}}[\hat{P}_f^\star] = \frac{\mathbb{E}_{\mathcal{X}}\left[\sqrt{\Phi\left(\frac{-\mathbb{E}_{\mathcal{D}}[\hat{g}(\boldsymbol{x})]}{\sqrt{\mathbb{V}_{\mathcal{D}}[\hat{g}(\boldsymbol{x})]}}\right)\Phi\left(\frac{\mathbb{E}_{\mathcal{D}}[\hat{g}(\boldsymbol{x})]}{\sqrt{\mathbb{V}_{\mathcal{D}}[\hat{g}(\boldsymbol{x})]}}\right)}\right]}{\mathbb{E}_{\mathcal{X}}\left[\Phi\left(\frac{-\mathbb{E}_{\mathcal{D}}[\hat{g}(\boldsymbol{x})]}{\sqrt{\mathbb{V}_{\mathcal{D}}[\hat{g}(\boldsymbol{x})]}}\right)\right]}. \tag{16}$$

Once the GP model becomes enough accurate, $\kappa^\star$ should be very small. Herein, the stopping criterion is defined by $\kappa^\star < \varepsilon$, where ε is a user-specified threshold.

Failure probability function estimation by Imprecise Augmented Stochastic Simulation (IASS)

In this subsection, we will consider the case that $\boldsymbol{\theta}$ is no longer a fixed value, but a vector of intervals. Accordingly, $P(\boldsymbol{\theta})$, as defined in Eq. (1), is not a deterministic value any more, but a function of interval variables. For instrumental purposes, all the distribution parameters are treated as random variables in the following. That is, we assume an auxiliary probability distribution for each interval variable of $\boldsymbol{\theta}$. Note that this assumption does not imply that $\boldsymbol{\theta}$ must be a random vector in nature, but just serves as an instrumental tool for performing the proposed method. Let

the auxiliary joint PDF and CDF of $\boldsymbol{\theta}$ be denoted as $\varphi(\boldsymbol{\theta}) = \prod_{j=1}^{d} \varphi_j(\theta_j)$ and $\Phi(\boldsymbol{\theta}) = \prod_{j=1}^{d} \Phi_j(\theta_j)$ respectively, where $\varphi_j(\theta_j)$ and $\Phi_j(\theta_j)$ are the marginal PDF and CDF of θ_j respectively.

The random vector $\boldsymbol{x}$ is called ***aleatory uncertainty vector*** as the aleatory uncertainty of model inputs is represented by means of its probability characterization, and the corresponding random-variate space $\mathcal{X}$ is termed as ***aleatory uncertainty space***. Under the previous assumption, we shall refer to the random vector $\boldsymbol{\theta}$ as ***epistemic uncertainty vector*** and the associated support Θ as ***epistemic uncertainty space***, respectively, since $\boldsymbol{\theta}$ characterizes the epistemic uncertainty of distribution parameters of $\boldsymbol{x}$ due to the lack of information. Consider an ***augmented uncertainty vector*** $\boldsymbol{v} = [\boldsymbol{x}, \boldsymbol{\theta}]$, i.e., a composition of aleatory uncertainty vector and epistemic uncertainty vector, whose joint PDF and ***augmented uncertainty space*** are denoted as $w(\boldsymbol{v}) = f(\boldsymbol{x}|\boldsymbol{\theta})\varphi(\boldsymbol{\theta})$ and $\mathcal{V} = \mathcal{X} \oplus \Theta$ respectively. Therefore, the failure probability function defined in Eq. (1) can be rewritten as:

$$\begin{aligned} P_f(\boldsymbol{\theta}) &= \int_{\mathcal{V}} I_F(\boldsymbol{v}) w(\boldsymbol{v}') \mathrm{d}\boldsymbol{v}' \\ &= \int_{\Theta} \int_{\mathcal{X}} I_F(\boldsymbol{v}) f(\boldsymbol{x}|\boldsymbol{\theta}) \varphi(\boldsymbol{\theta}') \mathrm{d}\boldsymbol{x} \mathrm{d}\boldsymbol{\theta}' \\ &= \int_{\mathcal{X}} I_F(\boldsymbol{v}) f(\boldsymbol{x}|\boldsymbol{\theta}) \mathrm{d}\boldsymbol{x}, \end{aligned} \tag{17}$$

where $\boldsymbol{v}' = [\boldsymbol{x}, \boldsymbol{\theta}']$; $\boldsymbol{\theta}'$ is i.i.d. with $\boldsymbol{\theta}$; $I_F(\boldsymbol{v})$ is the augmented failure indicator function corresponding to the augmented g-function $g(\boldsymbol{v})$. With Eq. (17), the failure indicator function is extended to the augmented uncertainty space, while it is noted that the integral is only with respect to $\boldsymbol{x}$. This treatment can bring several benefits, which will be discussed later. However, it is still tricky to evaluate the functional form of $P_f(\boldsymbol{\theta})$ with respect to the full vector $\boldsymbol{\theta}$ due to the underling complexity.

Alternatively, the random-sampling high-dimensional model representation (RS-HDMR) (Li et al. 2002) is adopted to decompose the original FPF into a summation of component functions of increasing orders such that:

$$P_{f,\mathrm{RS}}(\boldsymbol{\theta}) = P_{f,\mathrm{RS},0} + \sum_{j=1}^{m} P_{f,\mathrm{RS},j}\left(\theta_j\right) + \sum_{j<k}^{m} P_{f,\mathrm{RS},jk}\left(\theta_j, \theta_k\right) + \cdots + P_{f,\mathrm{RS},1,\ldots,m}(\boldsymbol{\theta}), \tag{18}$$

in which $P_{f,\mathrm{RS},0}$ is a zeroth-order (constant) component, $P_{f,\mathrm{RS},j}\left(\theta_j\right)$ is a first-order component function of the distribution parameter θ_j, $P_{f,\mathrm{RS},jk}\left(\theta_j,\theta_k\right)$ is a second-order component function of the distribution parameters θ_j and θ_k, etc. According to Eq. (17), these RS-HDMR component functions can be further derived as:

$$\begin{aligned} P_{f,\mathrm{RS},0} &= \int_{\Theta} P_f(\boldsymbol{\theta})\varphi(\boldsymbol{\theta})\mathrm{d}\boldsymbol{\theta} \\ &= \int_{\Theta}\int_{\mathcal{X}} I_F(\boldsymbol{v}) f(\boldsymbol{x}|\boldsymbol{\theta})\varphi(\boldsymbol{\theta})\mathrm{d}\boldsymbol{x}\mathrm{d}\boldsymbol{\theta} \\ &= \int_{\mathcal{V}} I_F(\boldsymbol{v})\omega(\boldsymbol{v})\mathrm{d}\boldsymbol{v} \\ &= \mathbb{E}_{\mathcal{V}}[I_F(\boldsymbol{v})], \end{aligned} \tag{19}$$

$$\begin{aligned} P_{f,\mathrm{RS},j}\left(\theta_j\right) &= \int_{\Theta_{-j}} P_f(\boldsymbol{\theta})\varphi(\theta_j,\boldsymbol{\theta}_{-j})\mathrm{d}\boldsymbol{\theta}_{-j} - P_{f,\mathrm{RS},0} \\ &= \int_{\Theta_{-j}}\int_{\mathcal{X}} I_F(\boldsymbol{v}) f(\boldsymbol{x}|\boldsymbol{\theta})\varphi(\theta_j,\boldsymbol{\theta}_{-j})\mathrm{d}\boldsymbol{x}\mathrm{d}\boldsymbol{\theta}_{-j} - P_{f,\mathrm{RS},0} \\ &= \int_{\mathcal{V}_{-\Theta_j}} I_F(\boldsymbol{v})\omega(\theta_j,\boldsymbol{v}_{-\theta_j})\mathrm{d}\boldsymbol{v}_{-\theta_j} - P_{f,\mathrm{RS},0} \\ &= \mathbb{E}_{\mathcal{V}_{-\Theta_j}}[I_F(\boldsymbol{v}|\theta_j,\boldsymbol{v}_{-\theta_j})] - P_{f,\mathrm{RS},0}, \end{aligned} \tag{20}$$

$$\begin{aligned} P_{f,\mathrm{RS},jk}\left(\theta_j,\theta_k\right) &= \int_{\Theta_{-jk}} P_f(\boldsymbol{\theta})\varphi(\theta_j,\theta_k,\boldsymbol{\theta}_{-jk})\mathrm{d}\boldsymbol{\theta}_{-jk} - P_{f,\mathrm{RS},j}\left(\theta_j\right) - P_{f,\mathrm{RS},k}\left(\theta_k\right) - P_{f,\mathrm{RS},0} \\ &= \int_{\Theta_{-jk}}\int_{\mathcal{X}} I_F(\boldsymbol{v}) f(\boldsymbol{x}|\boldsymbol{\theta})\varphi(\theta_j,\theta_k,\boldsymbol{\theta}_{-jk})\mathrm{d}\boldsymbol{x}\mathrm{d}\boldsymbol{\theta}_{-jk} - P_{f,\mathrm{RS},j}\left(\theta_j\right) - P_{f,\mathrm{RS},k}\left(\theta_k\right) - P_{f,\mathrm{RS},0} \\ &= \int_{\mathcal{V}_{-\Theta_{jk}}} I_F(\boldsymbol{v})\omega(\theta_j,\theta_k,\boldsymbol{v}_{-(\theta_j,\theta_k)})\mathrm{d}\boldsymbol{v}_{-(\theta_j,\theta_k)} - P_{f,\mathrm{RS},j}\left(\theta_j\right) - P_{f,\mathrm{RS},k}\left(\theta_k\right) - P_{f,\mathrm{RS},0} \\ &= \mathbb{E}_{\mathcal{V}_{-\Theta_{jk}}}\left[I_F(\boldsymbol{v}|\theta_j,\theta_k,\boldsymbol{v}_{-(\theta_j,\theta_k)})\right] - P_{f,\mathrm{RS},j}\left(\theta_j\right) - P_{f,\mathrm{RS},k}\left(\theta_k\right) - P_{f,\mathrm{RS},0}, \end{aligned} \tag{21}$$

where $\boldsymbol{\theta}_{-j}$ denotes the epistemic uncertainty vector excluding θ_j, $\boldsymbol{v}_{-\theta_j}$ denotes the augmented uncertainty vector excluding θ_j, $\boldsymbol{\theta}_{-jk}$ denotes the epistemic uncertainty vector excluding θ_j and θ_k, $\boldsymbol{v}_{-(\theta_j,\theta_k)}$ denotes the augmented uncertainty vector excluding θ_j and θ_k. Previous studies indicate that the high-order terms in the expansion often are negligible for many realistic problems (Wei et al. 2019a; Wei et al. 2019b), and only the truncation up to the second order is considered in this work, but any higher-order RS-HDMR component function can be similarly derived if necessary.

Within the RS-HDMR framework, one can notice that the main task now is to evaluate the low-order component functions for approximating the FPF. By using Eq. (17), the RS-HDMR component functions are further converted to the integrals with respect to the augmented uncertainty vector of decreasing dimensions. This conversation is useful since the two-fold integrals are equivalently transformed to be one-fold ones, which will reduce the computational complexity substantially. Besides, the computational efficiency for inferring these component functions is also improved if we apply the proposed ALPI by making full use of the correlation information revealed in both aleatory and epistemic uncertainty spaces.

For convenience, we can reformulate the second-order truncated RS-HDMR decomposition as:

$$P_{f,\mathrm{RS}}(\boldsymbol{\theta}) \approx \frac{(m-1)(m-2)}{2}\mathcal{P}_{f,\mathrm{RS},0} - (m-2)\sum_{j=1}^{m}\mathcal{P}_{f,\mathrm{RS},j}(\theta_j) + \sum_{j<k}^{m}\mathcal{P}_{f,\mathrm{RS},jk}(\theta_j,\theta_k), \tag{22}$$

where $\mathcal{P}_{f,\mathrm{RS},0} = P_{f,\mathrm{RS},0} = \mathbb{E}_{\mathcal{V}}[I_F(\boldsymbol{v})]$, $\mathcal{P}_{f,\mathrm{RS},j}(\theta_j) = \mathbb{E}_{\mathcal{V}_{-\Theta_j}}[I_F(\boldsymbol{v}|\theta_j,\boldsymbol{v}_{-\theta_j})]$ and $\mathcal{P}_{f,\mathrm{RS},jk}(\theta_j,\theta_k) = \mathbb{E}_{\mathcal{V}_{-\Theta_{jk}}}\left[I_F(\boldsymbol{v}|\theta_j,\theta_k,\boldsymbol{v}_{-(\theta_j,\theta_k)})\right]$. The constant component $\mathcal{P}_{f,\mathrm{RS},0}$ or $P_{f,\mathrm{RS},0}$ is also referred to as ***augmented failure probability*** since it integrates over the augmented uncertainty vector (see Eq. (19)). This reformulation is useful since one can easily derive the upper bound variance of the first-order and second-order component functions when implementing the ALAPI method (see Eqs. (36)-(37)). In this setting, the main focus is to evaluate the component functions in Eq. (22), and one should not be confused with the component functions defined in Eq. (18). Obviously, the crude Monte Carlo simulation (MCS) can be directly used to estimate those RS-HDMR components both in Eqs. (18) and (22). For example, the estimators for those components in Eq. (22) can be given by:

$$\hat{\mathcal{P}}_{f,\mathrm{RS},0} = \frac{1}{N}\sum_{s=1}^{N} I_F(\boldsymbol{v}^{(s)}), \tag{23}$$

$$\hat{\mathcal{P}}_{f,\mathrm{RS},j}\left(\theta_j\right) = \frac{1}{N}\sum_{s=1}^{N} I_F((\boldsymbol{v}|\theta_j,\boldsymbol{\theta}_{-j})^{(s)}), \tag{24}$$

$$\hat{\mathcal{P}}_{f,\mathrm{RS},jk}\left(\theta_j,\theta_k\right) = \frac{1}{N}\sum_{s=1}^{N} I_F((\boldsymbol{v}|\theta_j,\theta_k,\boldsymbol{\theta}_{-jk})^{(s)}), \tag{25}$$

where $\{\boldsymbol{v}^{(s)}\}_{s=1}^{N}$, $\{(\boldsymbol{v}|\theta_j,\boldsymbol{\theta}_{-j})^{(s)}\}_{s=1}^{N}$ and $\{(\boldsymbol{v}|\theta_j,\theta_k,\boldsymbol{\theta}_{-jk})^{(s)}\}_{s=1}^{N}$ given fixed θ_j and θ_k are three sets of N simple random samples generated from $w(\boldsymbol{v})$, $w(\boldsymbol{v}|\theta_j,\boldsymbol{\theta}_{-j})$ and $w(\boldsymbol{v}|\theta_j,\theta_k,\boldsymbol{\theta}_{-jk})$, respectively. It is easy to prove that the above estimators are all unbiased, so we simply omit the proofs. Their variances can also be derived as:

$$\mathbb{V}_{\mathcal{V}}\left[\hat{\mathcal{P}}_{f,\mathrm{RS},0}\right]=\frac{1}{(N-1)N}\sum_{s=1}^{N}\left[I_F(\boldsymbol{v}^{(s)})-\hat{\mathcal{P}}_{f,\mathrm{RS},0}\right]^2, \tag{26}$$

$$\mathbb{V}_{\mathcal{V}_{-\Theta_j}}\left[\hat{\mathcal{P}}_{f,\mathrm{RS},j}\left(\theta_j\right)\right]=\frac{1}{(N-1)N}\sum_{s=1}^{N}\left[I_F((\boldsymbol{v}|\theta_j,\boldsymbol{\theta}_{-j})^{(s)})-\hat{\mathcal{P}}_{f,\mathrm{RS},j}\left(\theta_j\right)\right]^2, \tag{27}$$

$$\mathbb{V}_{\mathcal{V}_{-\Theta_{jk}}}\left[\hat{\mathcal{P}}_{f,\mathrm{RS},jk}\left(\theta_j,\theta_k\right)\right]=\frac{1}{(N-1)N}\sum_{s=1}^{N}\left[I_F((\boldsymbol{v}|\theta_j,\theta_k,\boldsymbol{\theta}_{-jk})^{(s)})-\hat{\mathcal{P}}_{f,\mathrm{RS},jk}\left(\theta_j,\theta_k\right)\right]^2. \tag{28}$$

When the sample size is large, the central limit theorem indicates that the sampling distributions of $\hat{\mathcal{P}}_{f,\mathrm{RS},0}$, $\hat{\mathcal{P}}_{f,\mathrm{RS},j}\left(\theta_j\right)$ and $\hat{\mathcal{P}}_{f,\mathrm{RS},jk}\left(\theta_j,\theta_k\right)$ approximately follow normal distributions. Therefore, their confidence intervals (CIs) can be derived by using the t interval. For example, the $(1-\alpha)100\%$ CI of $\hat{\mathcal{P}}_{f,\mathrm{RS},0}$ can be given by:

$$\left[\hat{\mathcal{P}}_{f,\mathrm{RS},0}-t_{N-1}(\alpha/2)\sqrt{\mathbb{V}_{\mathcal{V}}\left[\hat{\mathcal{P}}_{f,\mathrm{RS},0}\right]},\hat{\mathcal{P}}_{f,\mathrm{RS},0}+t_{N-1}(\alpha/2)\sqrt{\mathbb{V}_{\mathcal{V}}\left[\hat{\mathcal{P}}_{f,\mathrm{RS},0}\right]}\right], \tag{29}$$

where $t_{N-1}(\alpha/2)$ denotes the $(1-\alpha/2)$-th percentile of a Student's t-distribution with $N-1$ degrees of freedom. It should be noted that the proposed RS-HDMR based technique for estimating the FPF is actually a double-loop procedure, which is termed as ***Imprecise Augmented Stochastic Simulation*** (IASS) in this work. The computational efficiency of the IASS still depends on the sample size N and the grid size of $\boldsymbol{\theta}$, and hence it can be merely used as a reference method for verifying other newly-developed methods. For further reducing the computational burden, the proposed ALPI method will be incorporated into the IASS framework in next subsection.

Numerical implementation procedure of ALAPI

By combining the ALPI with IASS, a novel method, namely ALAPI, is proposed to efficiently estimate the FPF. The basic procedure for numerical implementation of the proposed method in-

cludes the following steps, which is also illustrated in Fig. 1.

Step 1: Generate a set of N simple random samples $\boldsymbol{V} = \{\boldsymbol{v}\}_{s=1}^{N}$ according to the augmented PDF $w(\boldsymbol{v})$, which serves as a sample pool for training a GP model for the augmented g-function $g(\boldsymbol{v})$. For this purpose, the auxiliary PDF $\varphi(\boldsymbol{\theta})$ for $\boldsymbol{\theta}$ should be specified in advance. In order to enable those points within the intervals to have the same chance of being sampled, we assume a uniform auxiliary PDF over its support for each θ_j in this work;

Step 2: Randomly select N_0 (e.g., $N_0 = 12$) samples among $\boldsymbol{V}$ and compute the corresponding augmented g-function values. An initial training sample set is then constructed by the N_0 input-output pairs, which is denoted as $\mathcal{T}$;

Step 3: Train or update a GP model, denoted as $\hat{g}(\boldsymbol{v})$, for the augmented g-function $g(\boldsymbol{v})$ based on $\mathcal{T}$. The Gaussian Process Regression toolbox in Matlab is used, and the mean function and covariance function are specified as the linear function and squared exponential kernel function respectively in this study;

Step 4: Compute the upper bound of posterior COV of augmented failure probability based on the trained GP model such that:

$$\kappa = \frac{\sum_{s=1}^{N} \sqrt{\Phi\left(\frac{-\mathbb{E}_{\mathcal{T}}[\hat{g}(\boldsymbol{v}^{(s)})]}{\sqrt{\mathbb{V}_{\mathcal{T}}[\hat{g}(\boldsymbol{v}^{(s)})]}}\right)\Phi\left(\frac{\mathbb{E}_{\mathcal{T}}[\hat{g}(\boldsymbol{v}^{(s)})]}{\sqrt{\mathbb{V}_{\mathcal{T}}[\hat{g}(\boldsymbol{v}^{(s)})]}}\right)}}{\sum_{s=1}^{N}\Phi\left(\frac{-\mathbb{E}_{\mathcal{T}}[\hat{g}(\boldsymbol{v}^{(s)})]}{\sqrt{\mathbb{V}_{\mathcal{T}}[\hat{g}(\boldsymbol{v}^{(s)})]}}\right)}. \tag{30}$$

If the stopping condition $\kappa < \varepsilon$ is satisfied, go to **Step 5**; otherwise, identify the point possessing maximum UPVC value among the sample pool $\boldsymbol{V}$ by

$$\boldsymbol{v}^{\star} = \arg\max_{\boldsymbol{v}\in\boldsymbol{V}} \mathrm{UPVC}(\boldsymbol{v}) = \arg\max_{\boldsymbol{v}\in\boldsymbol{V}} \Phi\left(\frac{-\mathbb{E}_{\mathcal{T}}[\hat{g}(\boldsymbol{v}^{(s)})]}{\sqrt{\mathbb{V}_{\mathcal{T}}[\hat{g}(\boldsymbol{v}^{(s)})]}}\right)\Phi\left(\frac{\mathbb{E}_{\mathcal{T}}[\hat{g}(\boldsymbol{v}^{(s)})]}{\sqrt{\mathbb{V}_{\mathcal{T}}[\hat{g}(\boldsymbol{v}^{(s)})]}}\right), \tag{31}$$

evaluate the corresponding g-function value $y^{\star} = g(\boldsymbol{v}^{\star})$, add $\{\boldsymbol{v}^{\star}, y^{\star}\}$ to the training sample set $\mathcal{T}$, and go to **Step 3**;

Step 5: Based on the well-trained GP model $\hat{g}(\boldsymbol{v})$, perform the IASS method to obtain a

estimate $\hat{P}_f(\boldsymbol{\theta})$ for the FPF. As defined in Eq. (22), each component function of RS-HDMR can also be inferred from the GP predictor. According to the ALPI method, the unbiased estimators for RS-HDMR component functions can be given by:

$$\hat{\mathcal{P}}_{f,\mathrm{RS},0} = \frac{1}{N}\sum_{s=1}^{N} \Phi\left(\frac{-\mathbb{E}_{\mathcal{T}}[\hat{g}(\boldsymbol{v}^{(s)})]}{\sqrt{\mathbb{V}_{\mathcal{T}}[\hat{g}(\boldsymbol{v}^{(s)})]}}\right), \tag{32}$$

$$\hat{\mathcal{P}}_{f,\mathrm{RS},j}\left(\theta_j\right) = \frac{1}{N}\sum_{s=1}^{N} \Phi\left(\frac{-\mathbb{E}_{\mathcal{T}}[\hat{g}((\boldsymbol{v}|\theta_j)^{(s)})]}{\sqrt{\mathbb{V}_{\mathcal{T}}[\hat{g}((\boldsymbol{v}|\theta_j)^{(s)})]}}\right), \tag{33}$$

$$\hat{\mathcal{P}}_{f,\mathrm{RS},jk}\left(\theta_j,\theta_k\right) = \frac{1}{N}\sum_{s=1}^{N} \Phi\left(\frac{-\mathbb{E}_{\mathcal{T}}[\hat{g}((\boldsymbol{v}|\theta_j,\theta_k)^{(s)})]}{\sqrt{\mathbb{V}_{\mathcal{T}}[\hat{g}((\boldsymbol{v}|\theta_j,\theta_k)^{(s)})]}}\right). \tag{34}$$

The upper bound of posterior variances of the component functions, which reflects the upper bound of the epistemic uncertainty due to the discretization error by using the ALAPI, can also be estimated by:

$$\overline{\mathbb{V}}_{\mathcal{T}}\left[\hat{\mathcal{P}}_{f,\mathrm{RS},0}\right] = \left[\frac{1}{N}\sum_{s=1}^{N}\sqrt{\Phi\left(\frac{-\mathbb{E}_{\mathcal{T}}[\hat{g}(\boldsymbol{v}^{(s)})]}{\sqrt{\mathbb{V}_{\mathcal{T}}[\hat{g}(\boldsymbol{v}^{(s)})]}}\right)\Phi\left(\frac{\mathbb{E}_{\mathcal{T}}[\hat{g}(\boldsymbol{v}^{(s)})]}{\sqrt{\mathbb{V}_{\mathcal{T}}[\hat{g}(\boldsymbol{v}^{(s)})]}}\right)}\right]^2, \tag{35}$$

$$\overline{\mathbb{V}}_{\mathcal{T}}\left[\hat{\mathcal{P}}_{f,\mathrm{RS},j}\left(\theta_j\right)\right] = \left[\frac{1}{N}\sum_{s=1}^{N}\sqrt{\Phi\left(\frac{-\mathbb{E}_{\mathcal{T}}[\hat{g}((\boldsymbol{v}|\theta_j)^{(s)})]}{\sqrt{\mathbb{V}_{\mathcal{T}}[\hat{g}((\boldsymbol{v}|\theta_j)^{(s)})]}}\right)\Phi\left(\frac{\mathbb{E}_{\mathcal{T}}[\hat{g}((\boldsymbol{v}|\theta_j)^{(s)})]}{\sqrt{\mathbb{V}_{\mathcal{T}}[\hat{g}((\boldsymbol{v}|\theta_j)^{(s)})]}}\right)}\right]^2, \tag{36}$$

$$\overline{\mathbb{V}}_{\mathcal{T}}\left[\hat{\mathcal{P}}_{f,\mathrm{RS},jk}\left(\theta_j,\theta_k\right)\right] = \left[\frac{1}{N}\sum_{s=1}^{N}\sqrt{\Phi\left(\frac{-\mathbb{E}_{\mathcal{T}}[\hat{g}((\boldsymbol{v}|\theta_j,\theta_k)^{(s)})]}{\sqrt{\mathbb{V}_{\mathcal{T}}[\hat{g}((\boldsymbol{v}|\theta_j,\theta_k)^{(s)})]}}\right)\Phi\left(\frac{\mathbb{E}_{\mathcal{T}}[\hat{g}((\boldsymbol{v}|\theta_j,\theta_k)^{(s)})]}{\sqrt{\mathbb{V}_{\mathcal{T}}[\hat{g}((\boldsymbol{v}|\theta_j,\theta_k)^{(s)})]}}\right)}\right]^2. \tag{37}$$

Note that this step does not require to evaluate on the original g-function, and then the computational burden can be alleviated significantly, especially for an expensive-to-evaluate computer simulator involved.

In the above steps, it should be emphasized that the user-specified threshold ε can affect the accuracy of resultant GP model, as well as the efficiency of the active learning process. Besides,

there is a possibility that the stopping condition is satisfied even though the GP model is indeed not accurate enough, e.g., at the early stage of training. To avoid this situation, one can simply use a delay judgment strategy, which means that the active learning process is stopped only when the stopping condition is satisfied for several times in succession (e.g., three). Besides, the estimators in Eqs. (32)-(34) are only unbiased for the GP model, but biased for the real g-function.

The proposed ALAPI method has three main attractive features, making it very efficient for estimating the FPF. First, by assuming an auxiliary PDF for the distribution parameter $\boldsymbol{\theta}$, the GP model is built in the joint aleatory and epistemic uncertainty space (i.e., the augmented uncertainty space). The spatial correlation information in the augmented uncertainty space is shown to be quite useful for the active learning process. Second, the discretization error is regarded as a kind of epistemic uncertainty via interpreting the failure probability integral from Bayesian inference, which enables to derive the upper bounds of posterior variances of the ALAPI estimators. Third, the proposed method is essentially a decoupled procedure through an elegant combination of the ALPI and IASS, yielding a major improvement in computational efficiency.

NUMERICAL EXAMPLES

In this section, three numerical examples are studied to verify the proposed method. Among the available state-of-the-art techniques for estimating the FPF, the active learning NISS developed in (Wei et al. 2019b) could be a potential competitor to the proposed method. Therefore, we mainly compare our method with this method by using the first numerical example. For notational clarity, we will denote this method simply as "NISS" below. One can refer to Appendix I for more detailed description of the NISS method used. In the third example, the ASS (Au 2005) is also implemented to evaluate the augmented failure probability (or constant RS-HDMR component). Besides, the developed IASS method is mainly adopted to provide reference results in all three numerical examples.

Example 1: a series system with four branches

The first example considers a series system with four branches, which has been extensively investigated in the context of precise probabilities (Echard et al. 2011; Cui and Ghosn 2019). The

performance function is given by:

$$y = g\left(x_1, x_2\right) = \min \begin{cases} 3 + \frac{(x_1 - x_2)^2}{10} - \frac{(x_1 + x_2)}{\sqrt{2}} \\ 3 + \frac{(x_1 - x_2)^2}{10} + \frac{(x_1 + x_2)}{\sqrt{2}} \\ (x_1 - x_2) + \frac{b}{\sqrt{2}} \\ (x_2 - x_1) + \frac{b}{\sqrt{2}} \end{cases}, \tag{38}$$

where b is a constant, specified as 4; The random variables x_1 and x_2 are normally distributed, denoted as $\mathcal{N}\left(\mu_1, \sigma_1^2\right)$ and $\mathcal{N}\left(\mu_2, \sigma_2^2\right)$ respectively. Due to the epistemic uncertainty, the distribution parameters (i.e., $\boldsymbol{\theta} = [\mu_1, \sigma_1, \mu_2, \sigma_2]$) are not deterministic, but uncertain. In this example, two cases by varying bounds of the distribution parameters are considered, as given in Tab. 1.

In the following, three methods, i.e., the proposed ALAPI, NISS and IASS, are employed to estimate the FPF. For both cases, the sample pool is constructed by 10^5 simple random samples for ALAPI and NISS, while the sample size for IASS is set to be 10^6. Besides, the threshold regarding the stopping condition is specified as $\varepsilon = 0.02$ for ALAPI.

Case I

For illustrating the active learning process of ALAPI, the upper bound of posterior COV of the augmented failure probability $\hat{\mathcal{P}}_{f,\mathrm{RS},0}$ (denoted as κ) against the number of adaptively added samples is plotted in Fig. 2a. It can be seen that as more samples are sequentially added into the initial training data set, the general trend of κ tends to decrease. Until the initial training sample set is enriched by a total number of 81 samples, the stopping condition of the active learning procedure is satisfied. Thus, this implies that only 93 performance function evaluations are required by the proposed ALAPI method, which are much less than the NISS method, say 164. The constant RS-HDMR calculated by the three methods are listed in the second to fourth rows of Tab. 2. As seen, the estimate given by IASS has a relatively small COV, and hence we are highly confident that this reference result should be very close to the true value. Compared to the reference result, both ALAPI and NISS are capable of yielding very desirable estimates for the constant-HDMR component in this case. Note that the accuracy of the proposed method can also be revealed by the

upper bound of posterior COV of $\hat{\mathcal{P}}_{f,\mathrm{RS},0}$ itself, given that the sampling variability for estimating $\overline{\mathbb{COV}}_{\mathcal{T}}[\hat{\mathcal{P}}_{f,\mathrm{RS},0}]$ is negligible. On the contrary, the COV (i.e., $\mathbb{COV}[\hat{\mathcal{P}}_{f,\mathrm{RS},0}]$) provided by the NISS method only accounts for the sampling variability. From Fig. 3a, one can also conclude that all the three methods are able to produce very accurate estimates for the four first-order RS-HDMR component functions. For limited space, only one second-order RS-HDMR component function computed by ALAPI and IASS is depicted in Fig. 4a. Remarkably, it is shown that the estimate by the proposed method accords well with that by the IASS, with the upper bound of posterior COV and COV being small.

In short, the proposed ALAPI method can offer comparable results against the NISS method, but requires less g-function evaluations in such a case with smaller epistemic uncertainty presented in the distribution parameters compared with case II.

Case II

In this case, the intervals for those distribution parameters are enlarged a little bit compared to case I, as shown in Tab. 1. The active learning process of the proposed ALAPI method is illustrated by the upper bound of posterior COV of the augmented failure probability against the number of adaptively added samples, as depicted in Fig. 2b. It is shown that the active learning process is convergent after the initial training sample set is enriched with 123 samples. That is, the proposed ALAPI only requires 135 g-function evaluations. As a comparison, 352 g-function calls are needed by the NISS method, which is about 2.6 times more than the proposed method. The constant RS-HDMR component computed by the three methods is listed in the fifth to seventh rows of Tab. 2. The estimate from IASS method can be taken as the "exact" value because its COV is extremely small. Clearly, the proposed method can produce a more close estimate to the "exact" value than the NISS method in this case. For the first-order RS-HDMR component functions shown in Fig. 3b, it can also be observed that the estimates $\hat{\mathcal{P}}_{\mathrm{RS},2}(\sigma_1)$ and $\hat{\mathcal{P}}_{\mathrm{RS},4}(\sigma_2)$ from the NISS method have larger errors than those by the proposed ALAPI method, by taking the results by IASS as reference. As shown in Fig. 4b, the proposed method can still offer a very accurate estimate of $\hat{\mathcal{P}}_{f,\mathrm{RS},13}\,(\mu_1,\mu_2)$ with a small upper bound of posterior COV.

To sum up, the proposed method still requires far less g-function calls than the NISS method, but the accuracy of the NISS method becomes worse as the intervals of the distribution parameters are enlarged in this case. Such phenomenon is consistent with what is reported in Ref. (Wei et al. 2021).

Example 2: a nonlinear oscillator

An undamped single-degree-of-freedom oscillator with nonlinear restoring force subject to rectangular pulse load (Bucher and Bourgund 1990) is adapted for the case of imprecise probability, which is shown in Fig. 5. The corresponding limit state function reads:

$$y = g\left(m, c_1, c_2, r, F_1, t_1\right) = 3r - \left| \frac{2F_1}{m(c_1+c_2)} \sin\left(\frac{t_1}{2}\sqrt{\frac{c_1+c_2}{m}}\right)\right|, \tag{39}$$

As listed in Tab. 3, six random variables are included in this example. Due to different levels of knowledge, the mean values are assumed to be deterministic, but the standard deviations are characterized by interval models.

For the ALAPI method, the sample pool is constructed with a set of 10^6 samples, and the threshold ε for the stopping condition is set to be 0.01. A number of 10^6 samples are used for IASS method. As shown in Fig. 6, the stopping condition indicates that the GP model is well-trained after a total number of 29 samples are adaptively added into the initial training data set. Therefore, the ALAPI method only requires 41 performance function evaluations in this example, even though the stopping criteria is somehow strict. Tab. 4 lists the constant RS-HDMR component estimated by ALAPI and IASS, where it is found that the results of both methods are in good agreement with each other, and process a quite small upper bound of posterior COV or COV. Thus, we can conclude that both methods offer fairly good estimates for $\hat{\mathcal{P}}_{f,\mathrm{RS},0}$. As shown in Figs. 7 and 8, the first- and second-order RS-HDMR components are also computed with high accuracy by ALAPI and IASS. Note that the higher-order component functions can also be computed on the basis of the trained GP model if necessary.

Example 3: a 120-bar space truss structure

As shown in Fig. 9, the third example consists of a 120-bar space truss structure, which has been extensively used as a benchmark in the context of design optimization of structures. In this case study, we would like to estimate the failure probability function when the structure is subjected to some uncertainties characterized by probability boxes, i.e., the Young's modulus of the material E, cross-sectional area A and applied load P. The detailed description of these variables is summarized in Tab. 5. The limit state function is defined as:

$$y = g(E, A, P) = \Delta - V(E, A, P), \tag{40}$$

where Δ is a threshold, specified as 55 mm; $V(E, A, P)$ is the vertical displacement of the top node, which is solved by a finite-element software, OpenSees.

The proposed ALAPI method is implemented to obtain the failure probability function $\hat{P}_f(\boldsymbol{\theta})$. The number of samples used to construct the sample pool and the threshold of the stopping criterion are set as 10^5 and 0.01, respectively. From Fig. 10, it can be found that the stopping criterion is reached after a total of 21 samples are added in the initial training data set. Therefore, the proposed method only needs 33 limit state function evaluations to train a GP model. From the GP model, the RS-HDMR component functions of the FPF can be inferred. For the constant RS-HDMR component, the proposed method is compared to the ASS and IASS. As summarized in Tab. 6, the proposed method is computationally much more saving compared to the other two methods in terms of the number of calls to the limit state function, but can still yield fairly good estimate. Fig. 11 shows the six first-order RS-HDMR component functions and their corresponding upper bound COVs. For limiting the length of our paper, only one second-order RS-HDMR component functions is given, as depicted in Fig. 12. From these RS-HDMR component functions, one can perform sensitivity analysis to determine the contribution of each single variable or variable pairs. These information is extremely useful for directing the future information collection so as to further reduce the epistemic uncertainty of the failure probability.

CONCLUSIONS

The main contribution of this work is to present a novel non-intrusive method, termed as *Active Learning Augmented Probabilistic Integration* (ALAPI), for efficiently estimating the failure probability function in the presence of imprecise probability models. Specifically, the probability-box models are taken as an example for characterizing aleatory uncertainty and epistemic uncertainty by a hierarchical structure. However, all the developments can be conveniently extended to the case with other imprecise probability models. For our purposes, an active learning probabilistic integration (ALPI) method is firstly presented by interpreting the failure probability integral with Bayesian inference, rather than a frequentist view. Further, a imprecise augmented stochastic simulation (IASS) method is proposed based on the ideas of RS-HDMR and augmented uncertainty space. Finally, the ALAPI is formed by a elegant combination of ALPI and IASS. The main feature of ALAPI is that the epistemic uncertainty resulted from discretization error is properly quantified and propagated from the computational pipelines, allowing properly qualifying the accuracy of RS-HDMR component functions of the FPF.

Three numerical examples are investigated to exemplify and validate the proposed method. It is shown that the proposed method can produce very accurate estimates of the RS-HDMR components up to a second order with a small number of g-function calls when the failure probability is relatively larger (typically, with $\hat{\mathcal{P}}_{f,\mathrm{RS},0} > 10^{-3}$). Besides, as revealed by Example 1 the proposed method could be not very sensitive to the level of epistemic uncertainty, which is in contrast to the NISS method. To make the paper concise, only the component functions are presented in the examples, but one can also easily compute the failure probability bounds or sensitivity indices based on the proposed method if interested (Wei et al. 2019a; Wei et al. 2019b).

While the findings are encouraging, the proposed method is still suffered from some limitations, e.g., small failure probabilities and high dimensions (in terms of the augmented uncertainty vector). These problems will be addressed in the future work.

DATA AVAILABILITY STATEMENT

Some or all data, models, or code that support the findings of this study are available from

the corresponding author upon reasonable request. (Matlab code of the proposed ALPI method, ALAPI method, IASS method and three numerical examples; OpenSees model of the 120-bar space truss structure in the third example.)

ACKNOWLEDGMENTS

The first author would like to appreciate the financial support from China Scholarship Council (CSC). The second author is grateful to the support from the National Natural Science Foundation of China (grant no. NSFC 51905430) and the Alexander von Humboldt Foundation. The second and forth authors would also like to show their thankfulness to the support of Mobility Program 2020 from Sino-German Center (grant number M-0175).

APPENDIX I. ACTIVE LEARNING NON-INTRUSIVE IMPRECISE STOCHASTIC SIMULATION

According to (Wei et al. 2019b), the active learning procedure can be injected into the general NISS framework so as to further reduce the computational burden. Depending on the HDMR used, two kinds of active learning NISS methods, i.e., AK-LEMCS-cut-HDMR and AK-GEMCS-RS-HDMR, have been developed. In the present study, we only compare AK-GEMCS-RS-HDMR with the proposed method, and hence only this method is revisited. Since the RS-HDMR component functions that need to be estimated in the proposed method are somewhat different from those in (Wei et al. 2019b), the original AK-GEMCS-RS-HDMR should be slightly modified for our purposes, and the revised procedures are briefly given as follows.

Step I.1: Generate a set of N simple random samples $\boldsymbol{V} = \{\boldsymbol{X}, \boldsymbol{S}\} = \{\boldsymbol{x}^{(s)}, \boldsymbol{\theta}^{(i)}\}_{i=1}^{N}$ from the augmented PDF $w(\boldsymbol{v})$, which serves as a sample pool for training a GP model for the g-function $g(\boldsymbol{x})$.

Step I.2: Randomly select N_0 (e.g., $N_0 = 12$) samples from $\boldsymbol{X}$, and compute the corresponding g-function values. Attribute these N_0 samples to the training sample set $\boldsymbol{Q}$.

Step I.3: Train or update the GP model, denoted as $\hat{g}(\boldsymbol{x})$, for the g-function $g(\boldsymbol{x})$ based on $\boldsymbol{Q}$.

Step I.4: Compute the GP predictions $\mathbb{E}_{\mathcal{Q}}[\hat{g}(\boldsymbol{x})]$ and $\mathbb{V}_{\mathcal{Q}}[\hat{g}(\boldsymbol{x})]$ based on the trained GP model $\hat{g}(\boldsymbol{x})$ for all the samples in $\boldsymbol{X}$, and judge whether the stopping condition is satisfied with the principle that $\min_{i=1}^{N} U(\boldsymbol{x}^{(i)}) \geq 2$, where $U(\boldsymbol{x}) = \frac{|\mathbb{E}_{\mathcal{Q}}[\hat{g}(\boldsymbol{x})]|}{\sqrt{\mathbb{V}_{\mathcal{Q}}[\hat{g}(\boldsymbol{x})]}}$. If the inequality is satisfied, go to **Step I.4**; otherwise, find the sample $\boldsymbol{x}^{\star}$ with the smallest U value among $\boldsymbol{X}$, compute the corresponding g-function value $y^{\star} = g(\boldsymbol{x}^{\star})$, add $\{\boldsymbol{x}^{\star}, y^{\star}\}$ to the training sample set $\mathcal{Q}$, and go to **Step I.3**;

Step I.4: Based on the well-trained GP model $\hat{g}(\boldsymbol{x})$, obtain a estimate $\hat{P}_f(\boldsymbol{\theta})$ for the FPF. The estimators for the RS-HDMR component functions defined in Eq. (22) are given by:

$$\hat{\mathcal{P}}_{f,\mathrm{RS},0} = \frac{1}{N}\sum_{i=1}^{N} \hat{I}_F(\boldsymbol{x}^{(i)}), \tag{A.1}$$

$$\hat{\mathcal{P}}_{f,\mathrm{RS},j}\left(\theta_j\right) = \frac{1}{N}\sum_{i=1}^{N} \hat{I}_F(\boldsymbol{x}^{(i)}) \frac{f(\boldsymbol{x}^{(i)}|\theta_j, \boldsymbol{\theta}_{-j}^{(i)})}{f(\boldsymbol{x}^{(i)}|\boldsymbol{\theta}^{(i)})}, \tag{A.2}$$

$$\hat{\mathcal{P}}_{f,\mathrm{RS},jk}\left(\theta_j, \theta_k\right) = \frac{1}{N}\sum_{i=1}^{N} \hat{I}_F(\boldsymbol{x}^{(i)}) \frac{f(\boldsymbol{x}^{(i)}|\theta_j, \theta_k, \boldsymbol{\theta}_{-jk}^{(i)})}{f(\boldsymbol{x}^{(i)}|\boldsymbol{\theta}^{(i)})}. \tag{A.3}$$

The sampling variability contained in the above estimators can be measured by the following variances:

$$\mathbb{V}\left[\hat{\mathcal{P}}_{f,\mathrm{RS},0}\right] = \frac{1}{(N-1)N}\sum_{i=1}^{N}\left[I_F(\boldsymbol{x}^{(\boldsymbol{i})}) - \hat{\mathcal{P}}_{f,\mathrm{RS},0}\right]^2, \tag{A.4}$$

$$\mathbb{V}\left[\hat{\mathcal{P}}_{f,\mathrm{RS},j}\left(\theta_j\right)\right] = \frac{1}{(N-1)N}\sum_{i=1}^{N}\left[\hat{I}_F(\boldsymbol{x}^{(i)}) \frac{f(\boldsymbol{x}^{(i)}|\theta_j, \boldsymbol{\theta}_{-j}^{(i)})}{f(\boldsymbol{x}^{(i)}|\boldsymbol{\theta}^{(i)})} - \hat{\mathcal{P}}_{f,\mathrm{RS},j}\left(\theta_j\right)\right]^2, \tag{A.5}$$

$$\mathbb{V}\left[\hat{\mathcal{P}}_{f,\mathrm{RS},jk}\left(\theta_j, \theta_k\right)\right] = \frac{1}{(N-1)N}\sum_{i=1}^{N}\left[\hat{I}_F(\boldsymbol{x}^{(i)}) \frac{f(\boldsymbol{x}^{(i)}|\theta_j, \theta_k, \boldsymbol{\theta}_{-jk}^{(i)})}{f(\boldsymbol{x}^{(i)}|\boldsymbol{\theta}^{(i)})} - \hat{\mathcal{P}}_{f,\mathrm{RS},jk}\left(\theta_j, \theta_k\right)\right]^2. \tag{A.6}$$

REFERENCES

Alvarez, D. A., Uribe, F., and Hurtado, J. E. (2018). "Estimation of the lower and upper bounds on the probability of failure using subset simulation and random set theory." *Mechanical Systems and Signal Processing*, 100, 782–801.

Au, S. (2005). "Reliability-based design sensitivity by efficient simulation." *Computers & Structures*, 83(14), 1048–1061.

Bae, S., Park, C., and Kim, N. H. (2020). "Estimating Effect of Additional Sample on Uncertainty Reduction in Reliability Analysis Using Gaussian Process." *Journal of Mechanical Design*, 142(11) 111706.

Beer, M., Ferson, S., and Kreinovich, V. (2013). "Imprecise probabilities in engineering analyses." *Mechanical Systems and Signal Processing*, 37(1-2), 4–29.

Briol, F.-X., Oates, C. J., Girolami, M., Osborne, M. A., Sejdinovic, D., et al.(2019). "Probabilistic integration: A role in statistical computation?." *Statistical Science*, 34(1), 1–22.

Bucher, C. G. and Bourgund, U. (1990). "A fast and efficient response surface approach for structural reliability problems." *Structural Safety*, 7(1), 57–66.

Buckley, J. J. (2005). *Fuzzy probabilities: new approach and applications*, Vol. 115. Springer Science & Business Media.

Cui, F. and Ghosn, M. (2019). "Implementation of machine learning techniques into the subset simulation method." *Structural Safety*, 79, 12–25.

Der Kiureghian, A. and Ditlevsen, O. (2009). "Aleatory or epistemic? does it matter?." *Structural Safety*, 31(2), 105–112.

Dubourg, V., Sudret, B., and Deheeger, F. (2013). "Metamodel-based importance sampling for structural reliability analysis." *Probabilistic Engineering Mechanics*, 33, 47–57.

Echard, B., Gayton, N., and Lemaire, M. (2011). "Ak-mcs: an active learning reliability method combining kriging and monte carlo simulation." *Structural Safety*, 33(2), 145–154.

Echard, B., Gayton, N., Lemaire, M., and Relun, N. (2013). "A combined importance sampling and kriging reliability method for small failure probabilities with time-demanding numerical

models." *Reliability Engineering & System Safety*, 111, 232–240.

Faes, M. and Moens, D. (2019). "Recent trends in the modeling and quantification of non-probabilistic uncertainty." *Archives of Computational Methods in Engineering*, 1–39.

Faes, M., Valdebenito, M., Yuan, X., Wei, P., and Beer, M. (2021a). "Augmented reliability analysis for estimating imprecise first excursion probabilities in stochastic linear dynamics." *Advances in Engineering Software*.

Faes, M. G., Valdebenito, M. A., Moens, D., and Beer, M. (2020). "Bounding the first excursion probability of linear structures subjected to imprecise stochastic loading." *Computers & Structures*, 239, 106320.

Faes, M. G., Valdebenito, M. A., Moens, D., and Beer, M. (2021b). "Operator norm theory as an efficient tool to propagate hybrid uncertainties and calculate imprecise probabilities." *Mechanical Systems and Signal Processing*, 152, 107482.

Jiang, C., Bi, R., Lu, G., and Han, X. (2013). "Structural reliability analysis using non-probabilistic convex model." *Computer Methods in Applied Mechanics and Engineering*, 254, 83–98.

Li, G., Wang, S.-W., and Rabitz, H. (2002). "Practical approaches to construct rs-hdmr component functions." *The Journal of Physical Chemistry A*, 106(37), 8721–8733.

Ling, C., Lu, Z., and Zhang, X. (2020). "An efficient method based on ak-mcs for estimating failure probability function." *Reliability Engineering & System Safety*, 106975.

Liu, H., Jiang, C., Jia, X., Long, X., Zhang, Z., and Guan, F. (2018). "A new uncertainty propagation method for problems with parameterized probability-boxes." *Reliability Engineering & System Safety*, 172, 64–73.

Liu, H., Jiang, C., Liu, J., and Mao, J. (2019). "Uncertainty propagation analysis using sparse grid technique and saddlepoint approximation based on parameterized p-box representation." *Structural and Multidisciplinary Optimization*, 59(1), 61–74.

Liu, W.-S. and Cheung, S. H. (2017). "Reliability based design optimization with approximate failure probability function in partitioned design space." *Reliability Engineering & System Safety*, 167, 602–611.

Möller, B. and Beer, M. (2004). *Fuzzy randomness: uncertainty in civil engineering and computational mechanics*. Springer Science & Business Media.

Murphy, K. P. (2012). *Machine learning: a probabilistic perspective*. MIT press.

O'Hagan, A. (1991). "Bayes–hermite quadrature." *Journal of Statistical Planning and Inference*, 29(3), 245–260.

Rasmussen, C. E. (2003). "Gaussian processes in machine learning." *Summer School on Machine Learning*, Springer, 63–71.

Rasmussen, C. E. and Ghahramani, Z. (2003). "Bayesian monte carlo." *Advances in Neural Information Processing Systems*, 505–512.

Sentz, K., Ferson, S., et al.(2002). *Combination of evidence in Dempster-Shafer theory*, Vol. 4015. Sandia National Laboratories Albuquerque.

Song, J., Valdebenito, M., Wei, P., Beer, M., and Lu, Z. (2020a). "Non-intrusive imprecise stochastic simulation by line sampling." *Structural Safety*, 84, 101936.

Song, J., Wei, P., Valdebenito, M., and Beer, M. (2020b). "Active learning line sampling for rare event analysis." *Mechanical Systems and Signal Processing*, 147, 107113.

Song, J., Wei, P., Valdebenito, M., and Beer, M. (2020c). "Adaptive reliability analysis for rare events evaluation with global imprecise line sampling." *Computer Methods in Applied Mechanics and Engineering*, 372, 113344.

Sun, S., Fu, G., Djordjević, S., and Khu, S.-T. (2012). "Separating aleatory and epistemic uncertainties: Probabilistic sewer flooding evaluation using probability box." *Journal of Hydrology*, 420, 360–372.

Wei, P., Liu, F., Lu, Z., and Wang, Z. (2018). "A probabilistic procedure for quantifying the relative importance of model inputs characterized by second-order probability models." *International Journal of Approximate Reasoning*, 98, 78–95.

Wei, P., Liu, F., Valdebenito, M., and Beer, M. (2021). "Bayesian probabilistic propagation of imprecise probabilities with large epistemic uncertainty." *Mechanical Systems and Signal Processing*, 149, 107219.

Wei, P., Lu, Z., and Song, J. (2014). "Extended monte carlo simulation for parametric global sensitivity analysis and optimization." *AIAA Journal*, 52(4), 867–878.

Wei, P., Song, J., Bi, S., Broggi, M., Beer, M., Lu, Z., and Yue, Z. (2019a). "Non-intrusive stochastic analysis with parameterized imprecise probability models: I. performance estimation." *Mechanical Systems and Signal Processing*, 124, 349–368.

Wei, P., Song, J., Bi, S., Broggi, M., Beer, M., Lu, Z., and Yue, Z. (2019b). "Non-intrusive stochastic analysis with parameterized imprecise probability models: II. reliability and rare events analysis." *Mechanical Systems and Signal Processing*, 126, 227–247.

Wei, P., Tang, C., and Yang, Y. (2019c). "Structural reliability and reliability sensitivity analysis of extremely rare failure events by combining sampling and surrogate model methods." *Proceedings of the Institution of Mechanical Engineers, Part O: Journal of Risk and Reliability*, 233(6), 943–957.

Wei, P., Zhang, X., and Beer, M. (2020). "Adaptive experiment design for probabilistic integration." *Computer Methods in Applied Mechanics and Engineering*, 365, 113035.

Yager, R. R. and Kreinovich, V. (1999). "Decision making under interval probabilities." *International Journal of Approximate Reasoning*, 22(3), 195–215.

Yuan, X., Faes, M. G., Liu, S., Valdebenito, M. A., and Beer, M. (2021). "Efficient imprecise reliability analysis using the augmented space integral." *Reliability Engineering & System Safety*, 107477.

Yuan, X., Zheng, Z., and Zhang, B. (2020). "Augmented line sampling for approximation of failure probability function in reliability-based analysis." *Applied Mathematical Modelling*, 80, 895–910.

Zhang, H. (2012). "Interval importance sampling method for finite element-based structural reliability assessment under parameter uncertainties." *Structural Safety*, 38, 1–10.

Zhang, H., Dai, H., Beer, M., and Wang, W. (2013). "Structural reliability analysis on the basis of small samples: an interval quasi-monte carlo method." *Mechanical Systems and Signal Processing*, 37(1-2), 137–151.

715 Zhang, H., Mullen, R. L., and Muhanna, R. L. (2010). “Interval monte carlo methods for structural
716 reliability.” *Structural Safety*, 32(3), 183–190.

List of Tables

Abbreviations

ALAPI active learning augmented probabilistic integration

ALPI active learning probabilistic integration

ASS augmented subset simulation

CDF cumulative distribution function

COV coefficient of variation

FPF failure probability function

GP Gaussian process

IASS imprecise augmented stochastic simulation

MCS Monte Carlo simulation

NIPI non-intrusive imprecise probabilistic integration

NISS non-intrusive imprecise stochastic simulation

p-box probability box

PDF probability density function

RMF response moment function

RS-HDMR random sampling high-dimensional representation model

UPVC upper bound posterior variance contribution

TABLE 1. Distribution parameters for Example 1.

Case	μ_1	σ_1	μ_2	σ_2
I	$[-0.5, 0.5]$	$[0.8, 1.2]$	$[-0.5, 0.5]$	$[0.8, 1.2]$
II	$[-0.8, 0.8]$	$[0.5, 1.5]$	$[-0.8, 0.8]$	$[0.5, 1.5]$

TABLE 2. Constant RS-HDMR component by different methods for Example 1.

Case	Method	$\hat{\mathcal{P}}_{f,\mathrm{RS},0}$	$\overline{\mathbb{COV}}_{\mathcal{T}}[\hat{\mathcal{P}}_{f,\mathrm{RS},0}]$ or $\mathbb{COV}[\hat{\mathcal{P}}_{f,\mathrm{RS},0}]$
I	ALAPI	0.0594	0.0172
	NISS	0.0589	0.0126
	IASS	0.0593	0.0040
II	ALAPI	0.0860	0.0186
	NISS	0.0855	0.0103
	IASS	0.0861	0.0033

TABLE 3. Statistical information of the random variables for Example 2.

Variable	Description	Distribution	Mean	Standard deviation
m	Mass	Normal	1.0	$\sigma_1 \in [0.02, 0.08]$
c_1	Stiffness of the first spring	Normal	1.0	$\sigma_2 \in [0.05, 0.15]$
c_2	Stiffness of the second spring	Normal	0.1	$\sigma_3 \in [0.005, 0.015]$
r	Yield displacement	Normal	0.5	$\sigma_4 \in [0.02, 0.08]$
F_1	Load amplitude	Lognormal	1.0	$\sigma_5 \in [0.10, 0.30]$
t_1	Load duration	Normal	1.0	$\sigma_6 \in [0.15, 0.25]$

TABLE 4. Constant RS-HDMR component by ALAPI and IASS for Example 2.

Method	$\hat{\mathcal{P}}_{f,\mathrm{RS},0}$	$\overline{\mathbb{COV}}_{\mathcal{T}}[\hat{\mathcal{P}}_{f,\mathrm{RS},0}]$ or $\mathbb{COV}[\hat{\mathcal{P}}_{f,\mathrm{RS},0}]$
ALAPI	0.0356	0.0100
IASS	0.0359	0.0052

TABLE 5. Statistical information of the random variables for Example 3.

Variable	Distribution	Mean	Standard deviation
E/Mpa	Normal	$\mu_E \in [2.10 \times 10^5, 2.20 \times 10^5]$	$\sigma_E \in [2.10 \times 10^4, 2.20 \times 10^4]$
A/mm	Normal	$\mu_A \in [1000, 1100]$	$\sigma_A \in [100, 110]$
P/kN	Lognormal	$\mu_P \in [500, 600]$	$\sigma_P \in [50, 60]$

TABLE 6. Constant RS-HDMR component by ALAPI, ASS and IASS for Example 3.

Method	$\hat{\mathcal{P}}_{f,\mathrm{RS},0}$	$\overline{\mathbb{COV}}_{\mathcal{T}}[\hat{\mathcal{P}}_{f,\mathrm{RS},0}]$ or $\mathbb{COV}[\hat{\mathcal{P}}_{f,\mathrm{RS},0}]$	N
ALAPI	0.0782	0.0004	33
ASS	0.0803	0.0938	3800
IASS	0.0754	0.0111	10^5

List of Figures

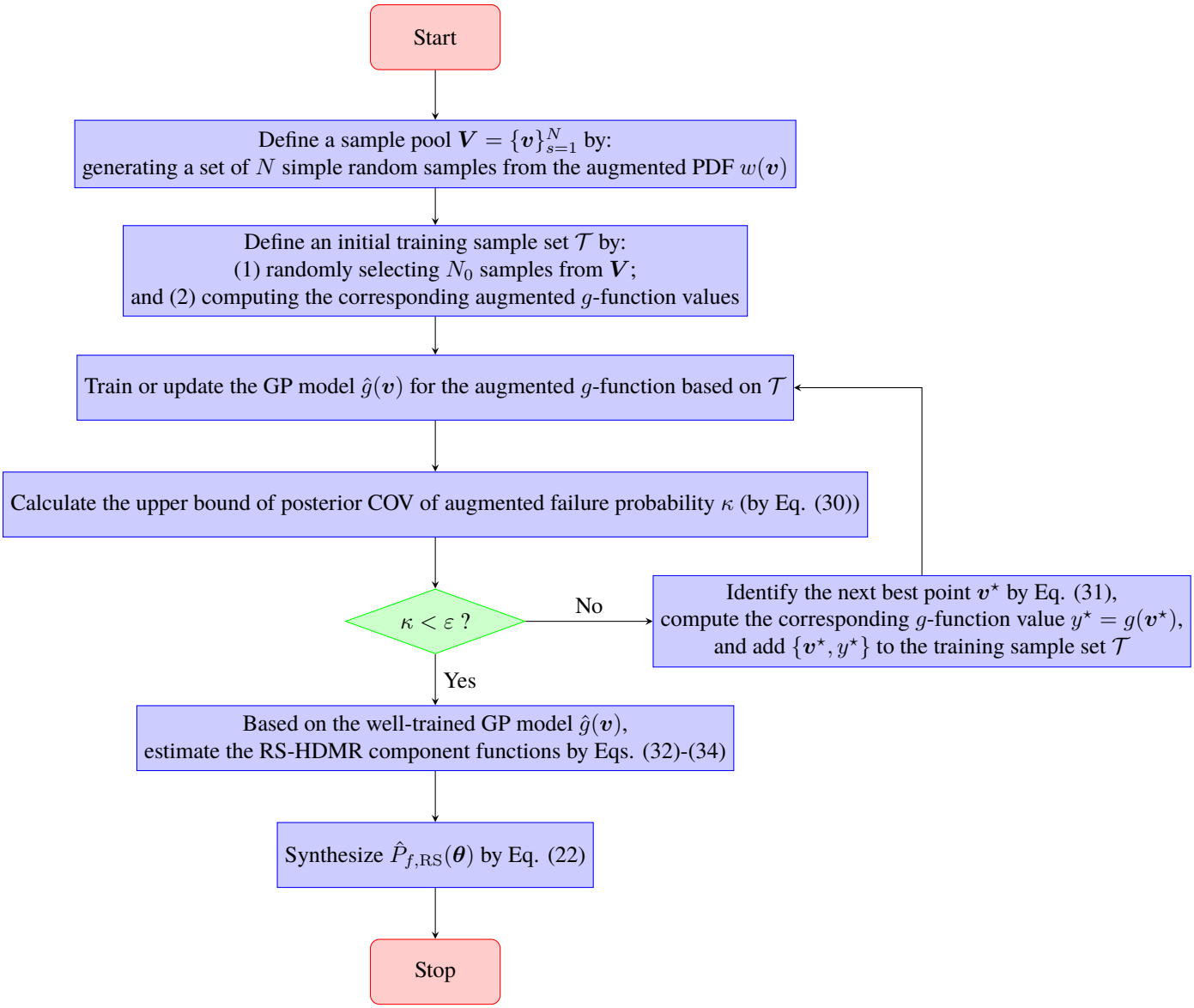

Fig. 1. Flowchart of the proposed ALAPI method.

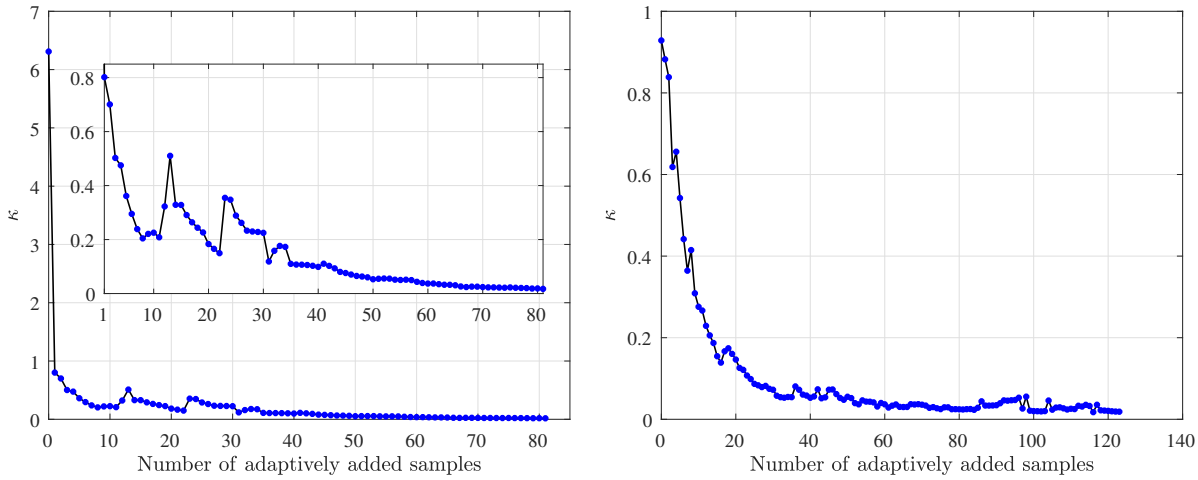

(a) Case I **(b)** Case II

Fig. 2. Upper bound of the posterior COV of $\hat{\mathcal{P}}_{f,\mathrm{RS},0}$ against the number of adaptively added samples for Example 1.

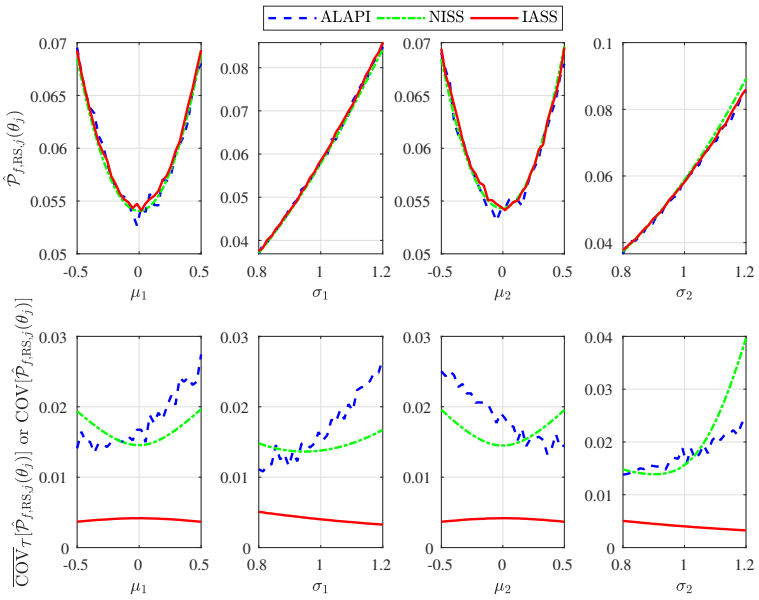

(a) Case I

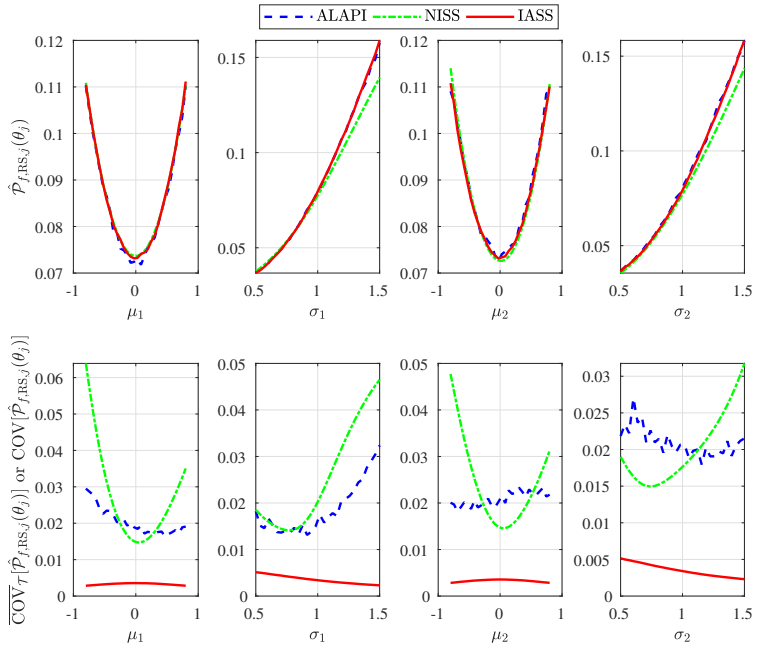

(b) Case II

Fig. 3. Four first-order RS-HDMR component functions for Example 1.

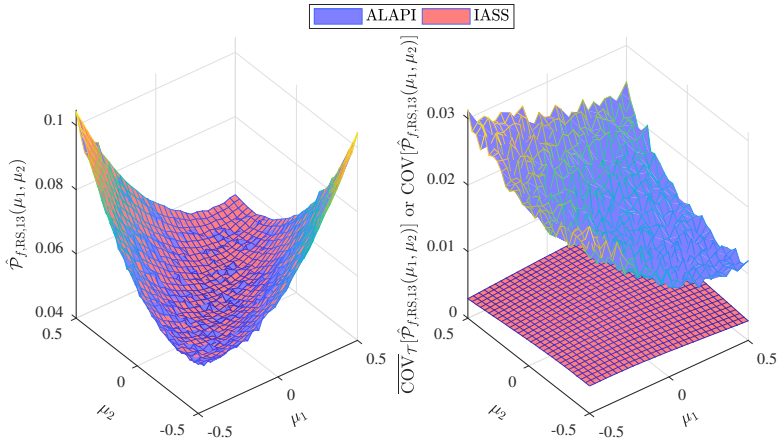

(a) Case I

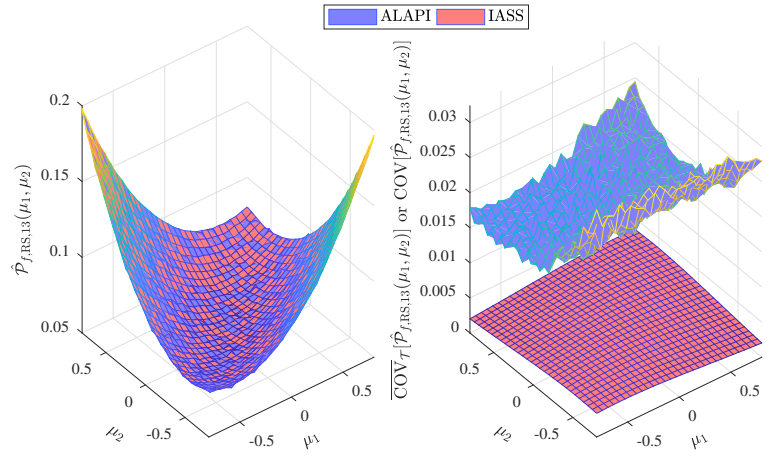

(b) Case II

Fig. 4. A second-order RS-HDMR component function for Example 1.

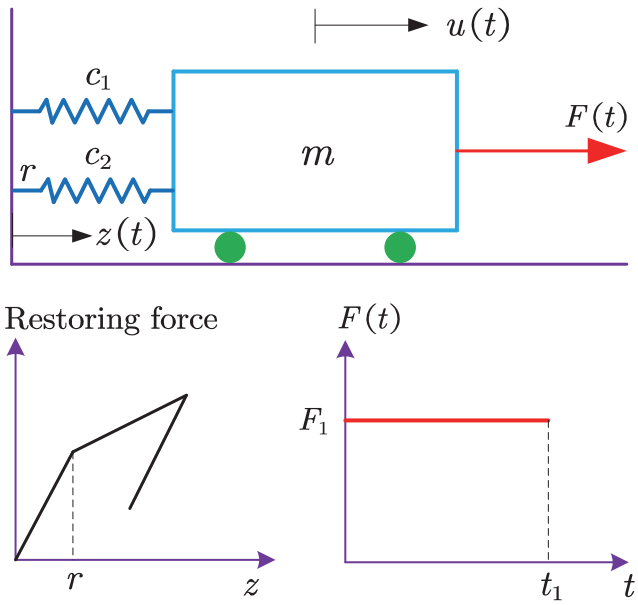

Fig. 5. An undamped SDOF oscillator with nonlinear restoring force subject to pulse load for Example 2.

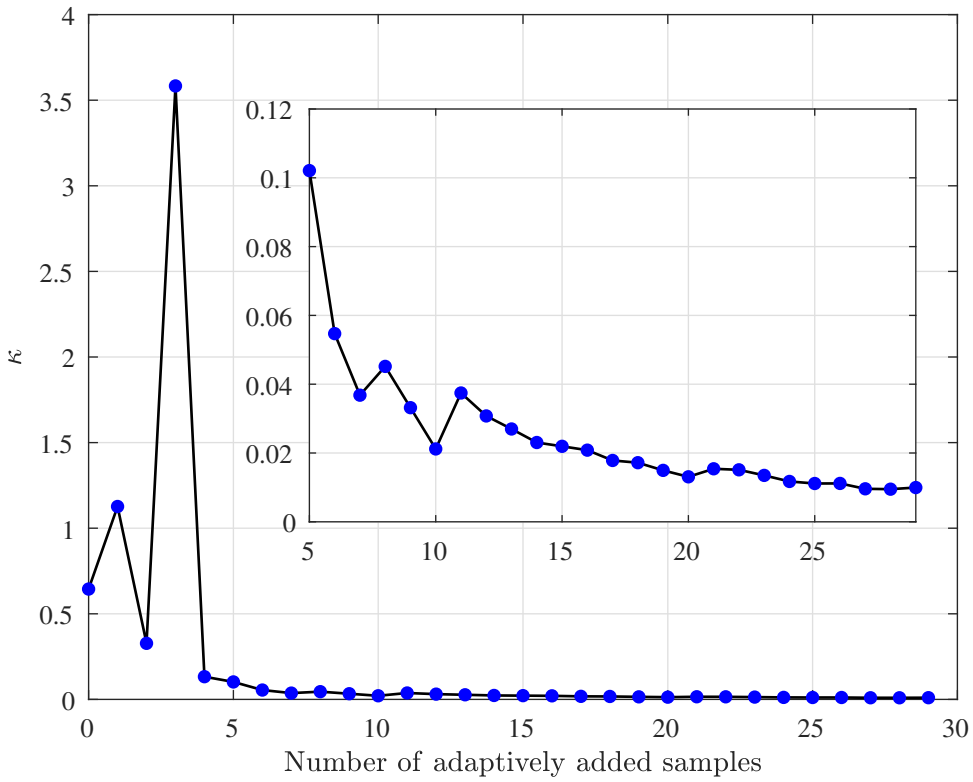

Fig. 6. Upper bound of the posterior COV of $\hat{\mathcal{P}}_{f,\mathrm{RS},0}$ against the number of adaptively added samples for Example 2.

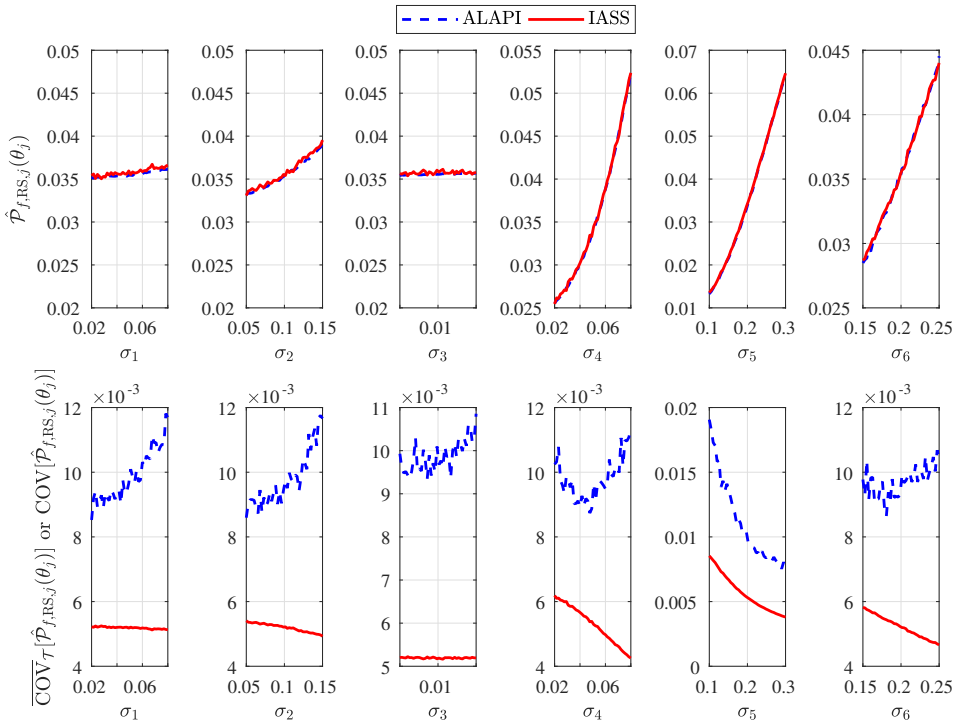

Fig. 7. Six first-order RS-HDMR component functions for Example 2.

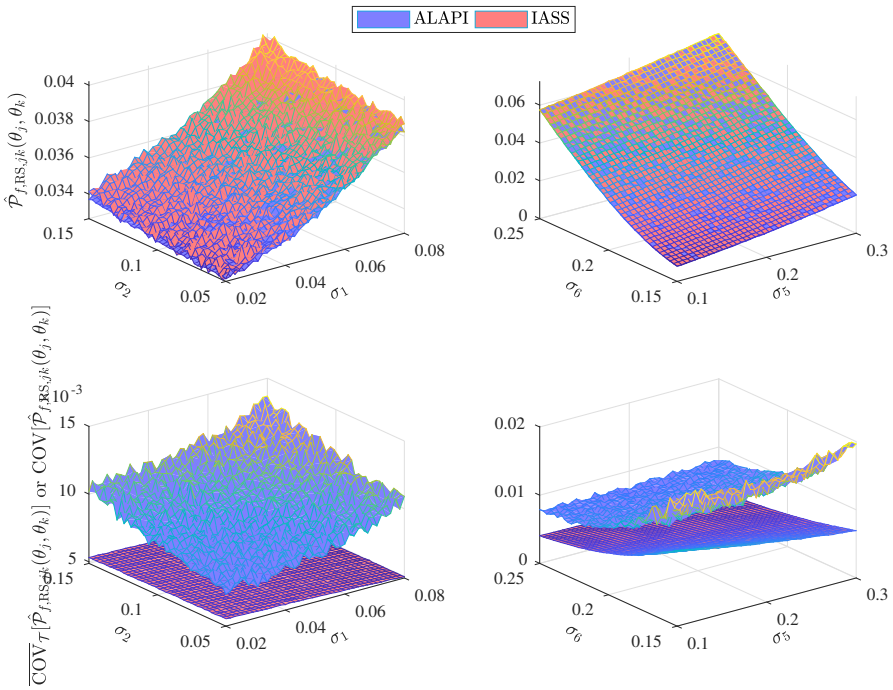

Fig. 8. Two second-order RS-HDMR component functions for Example 2.

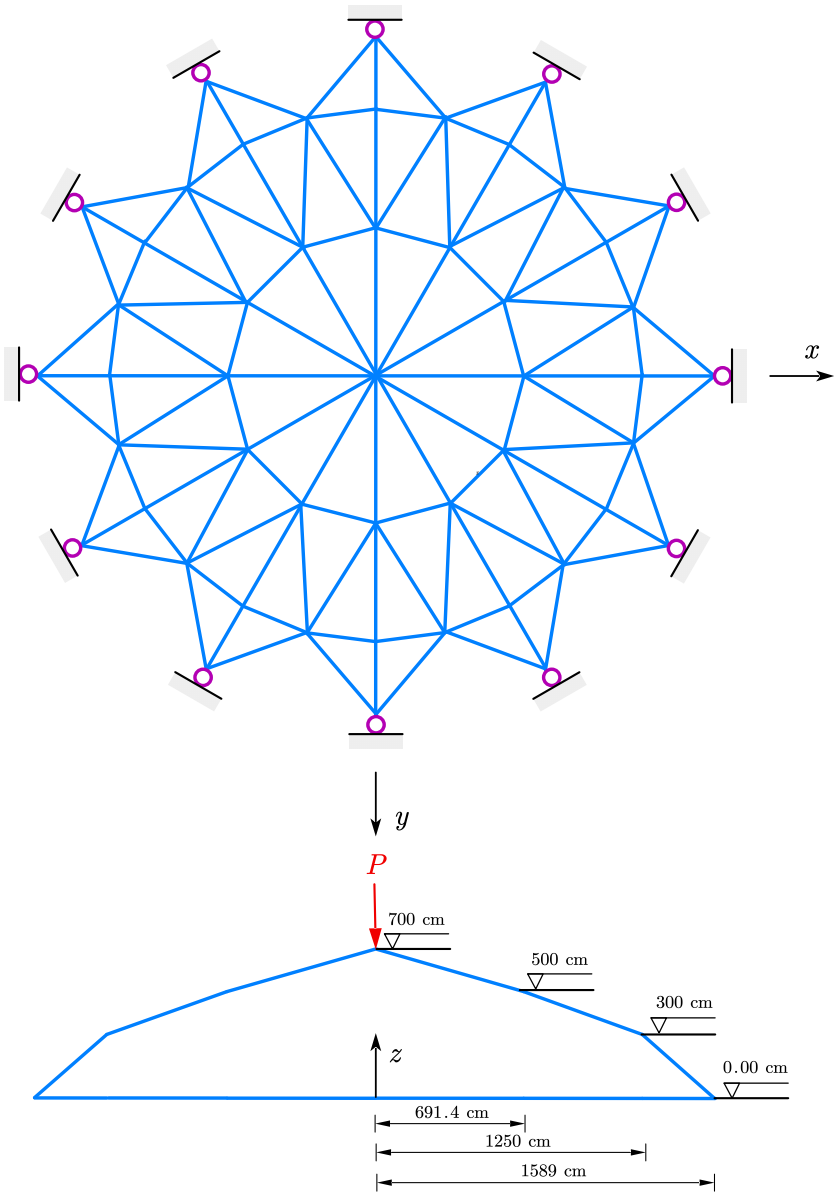

Fig. 9. A 120-bar space truss structure.

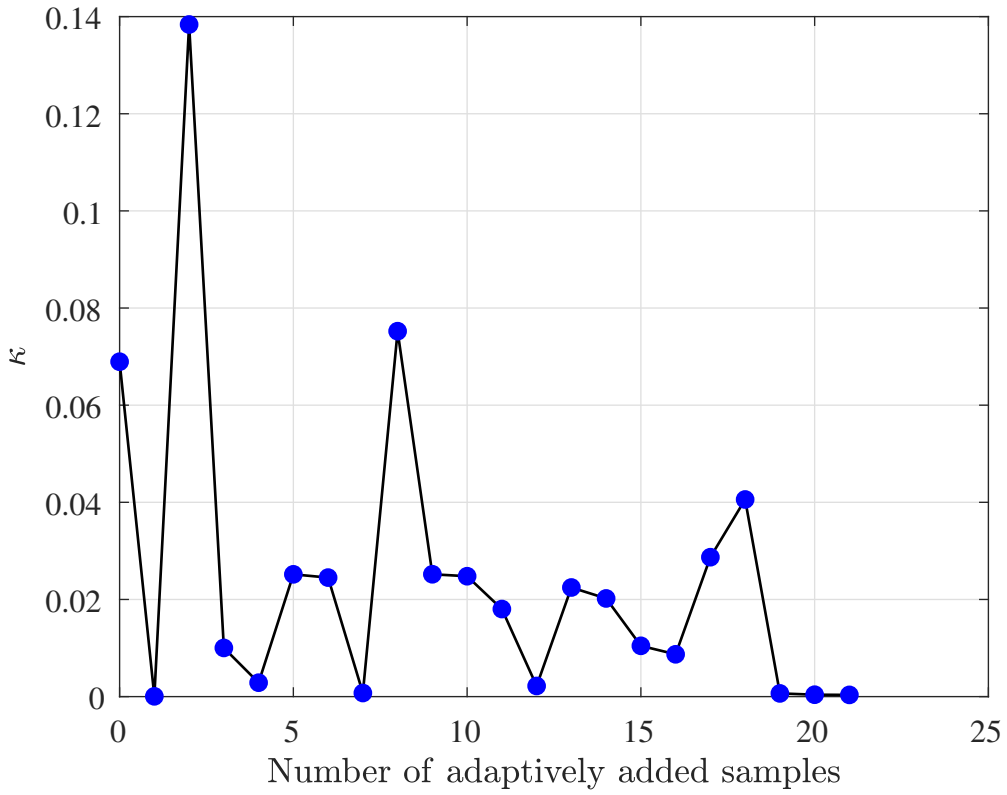

Fig. 10. Upper bound of the posterior COV of $\hat{\mathcal{P}}_{f,\mathrm{RS},0}$ against the number of adaptively added samples for Example 3.

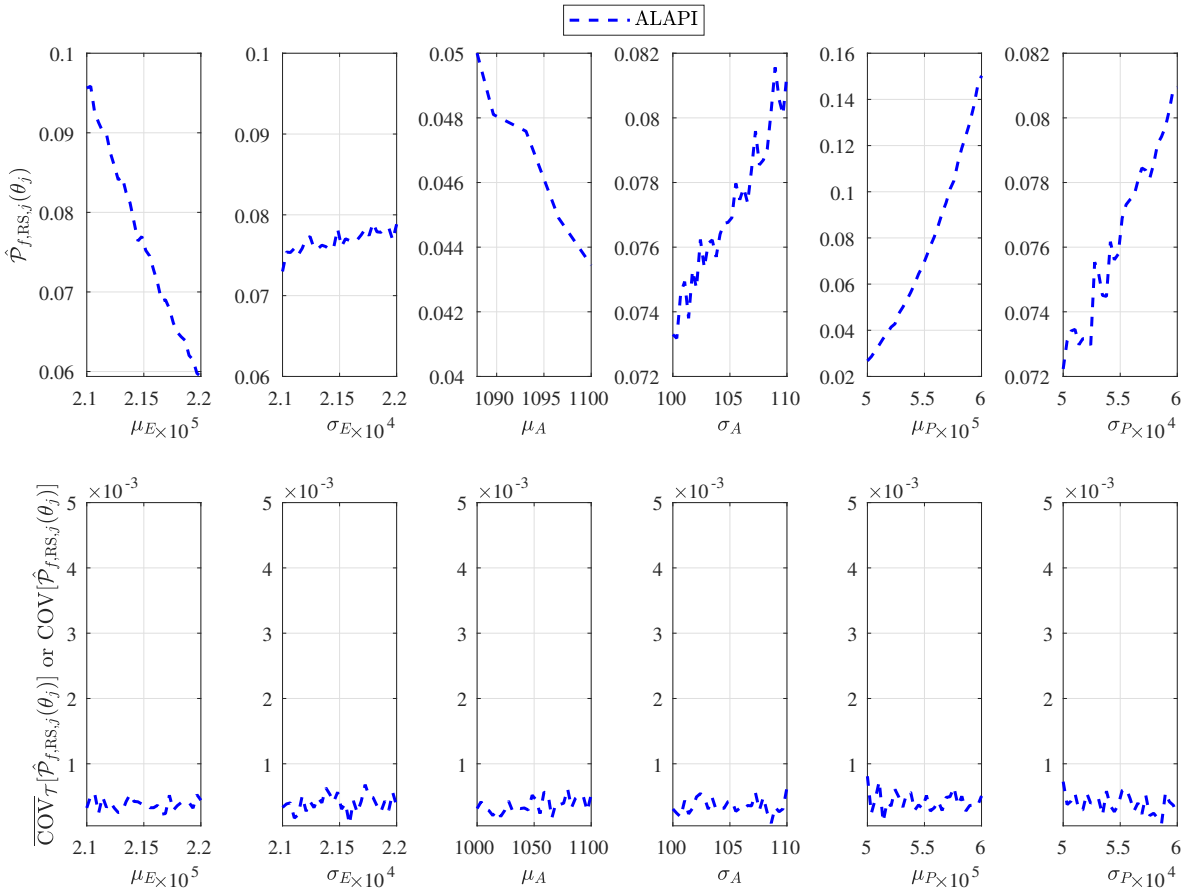

Fig. 11. Six first-order RS-HDMR component functions for Example 3.

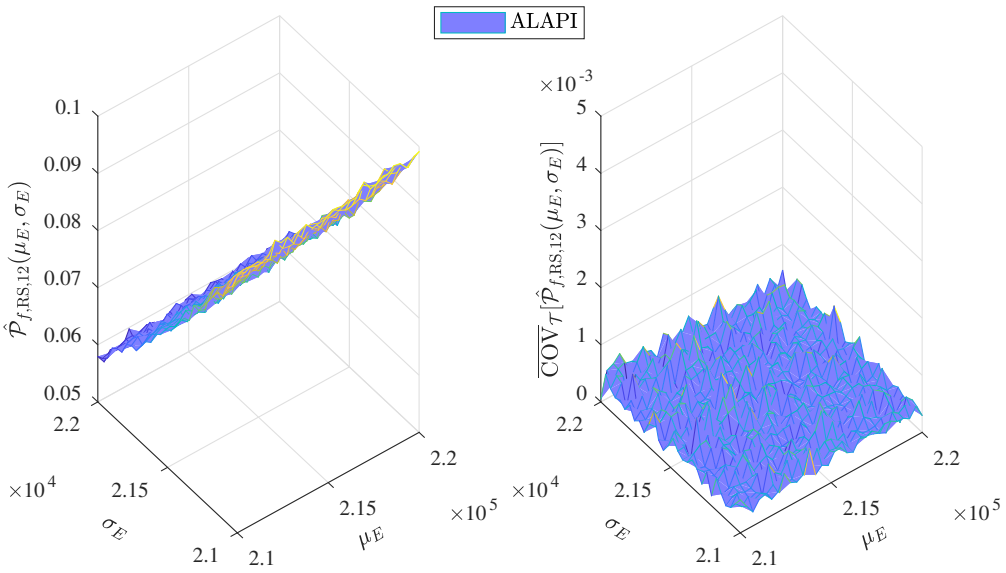

Fig. 12. One second-order RS-HDMR component function for Example 3.